University of Illinois at Urbana-Champaign

ACRC

Air Conditioning and Refrigeration Center A National Science Foundation/University Cooperative Research Center

Condensation of a 50/50 Blend of R-32/R-125 in Horizontal Tubes with and Without Oil

J. A. Gaibel, J. C. Chato, M. K. Dobson, M. Ponchner, P. J. Kenney,
R. L. Shimon, T. C. Villaneuva, N. L. Rhines, K. A. Sweeney,
D. G. Allen, and T. T. Hershberger

ACRC TR-56 May 1994

For additional information:

Air Conditioning and Refrigeration Center
University of Illinois
Mechanical & Industrial Engineering Dept.
1206 West Green Street
Urbana, IL 61801

(217) 333-3115

Effect of Geometric Variables and R-22 Alternatives on Refrigerant-Side Evaporation and Condensation
J. C. Chato, Principal Investigator

The Air Conditioning and Refrigeration Center was founded in 1988 with a grant from the estate of Richard W. Kritzer, the founder of Peerless of America Inc. A State of Illinois Technology Challenge Grant helped build the laboratory facilities. The ACRC receives continuing support from the Richard W. Kritzer Endowment and the National Science Foundation. The following organizations have also become sponsors of the Center.

Acustar Division of Chrysler
Allied Signal, Inc.
Amana Refrigeration, Inc.
Brazeway, Inc.
Carrier Corporation
Caterpillar, Inc.
E. I. duPont Nemours & Co.
Electric Power Research Institute
Ford Motor Company
Frigidaire Company
General Electric Company
Harrison Division of GM
ICI Americas, Inc.
Modine Manufacturing Company
Peerless of America, Inc.
Environmental Protection Agency
U.S. Army CERL
Whirlpool Corporation

For additional information:

Air Conditioning & Refrigeration Center
Mechanical & Industrial Engineering Dept.
University of Illinois
1206 West Green Street
Urbana, IL 61801

217 333 3115

Abstract

This study examined local condensation heat transfer and pressure drop for a pure 50/50% mixture of R-32/125 and for R-32/125 mixed with approximately 1%, 3%, and 5% concentrations of an ester oil. An apparatus was built to simulate conditions found in the condenser sections of domestic refrigerators/freezers. Experiments were performed to measure the internal heat transfer coefficients and pressure drops inside a 0.277 in. (7.0 mm) o.d. smooth, horizontal copper tube. It was observed from the oil samples that the oil concentration of the oil-refrigerant mixtures flowing through the test section changed for different mass fluxes and qualities. The data for the heat transfer coefficients were compared with existing correlations and the Dobson correlation demonstrated the best accuracy for the pure R-32/125 and predicted the performance of oil-refrigerant mixtures with less than 20% error when used with the Schlager enhancement factor. The experiments showed that oil addition degraded the heat transfer coefficient at vapor qualities greater than 50% and increased the pressure drop by as much as 25% at high mass fluxes.

Table of Contents

List of Figures

Page

List of Tables

Page

List of Variables and Symbols

A	Area	[m^2]
Bo	Bond Number, Eq. (2.4)	-----
C_p	Specific Heat at Constant Pressure	[kJ/kgK]
C_v	Specific Heat at Constant Volume	[kJ/kgK]
D	Diameter	[m]
D_{HYD}	Hydraulic Diameter	[m]
$EF_{s'/s}$	Correction Factor by Schlager et al., Eq. (2.35)	-----
f	Friction Factor	-----
F_1	Constant in Traviss et al. Correlation	-----
F_2	Constant in Traviss et al. Correlation	-----
Fr	Froude Number	-----
g	Downward Acceleration of Gravity	-----
G	Mass Flux	[kg/m^2s]
h	Heat Transfer Coefficient	[W/m^2K]
h	Enthalpy	[kJ/kg]
h_{fg}	Latent Heat of Vaporization	[kJ/kg]
h'_{fg}	Rohsenow's Modified Latent Heat of Vaporization	[kJ/kg]
Ja	Jakob Number, Eq. (2.4)	-----
k	Thermal Conductivity	[W/m K]
Nu	Nusselt Number	-----
P	Pressure	[kPa]
Pr	Prandtl Number, Eq. (2.4)	-----
P_r	Reduced Pressure, $P/P_{critical}$	-----
q	Heat	[W]
q"	Heat Flux	[W/m^2]
Re	Reynolds Number, Eq. (2.26)	-----
T	Temperature	[C]
u	Velocity	[m/s]
$u_{m,v}$	Mean Vapor Velocity	[m/s]
v	Specific Volume	[m^3/kg]
x	Quality	-----
X	Lockhart-Martinelli Parameter, Eqs. (2.12) and (2.28)	-----
y	Vertical Distance	[m]
z	Length	[m]
Z	Parameter Used in Shaw Correlation	-----
α	Thermal Diffusivity	[m^2/s]
α	Void Fraction	-----
δ	Film Thickness	[m]
ε_h	Eddy Diffusivity of Heat	[m^2/s]
ε_m	Eddy Diffusivity of Momentum	[m^2/s]
λ	Baker's Correction Factor, Eq. (2.1)	------
σ	Surface Tension	[N/m]
ψ	Baker's Correction Factor, Eq. (2.2)	-----

ϕ	Two-phase Multiplier, Eq. (2.20)	-----
θ_l	Liquid Level Angle, Eq. (2.20)	[rad]
μ	Dynamic Viscosity	[Pa s]
ν	Kinematic Viscosity	[m^2/s]
ρ	Density	[kg/m^3]
τ	Shear Stress	[N/m^2]
ω	Mass Fraction of refrigerant	-----
ω_o	Mass Fraction of oil	

Subscripts

a	Acceleration
eq	Equivalent Value for Liquid / Vapor Mixture
f	Fluid or Liquid
fg	Change from Liquid to Vapor
g	Gas or Vapor
htr	Heater
in	Inlet
l	Fluid or Liquid
m	Momentum Component
Nu	Based on Nusselt Number
out	Outlet
ref	Refrigerant
s	Surface
sat	Saturation Value
TP	Two-phase
v	Gas or Vapor
w	Wall
wat	Water
z	Distance along Tub

Chapter 1: Introduction

Two major issues facing the air-conditioning and refrigeration industries today are the elimination of halogenated chlorofluorocarbons (CFC's) and the increasingly strict energy efficiency requirements as mandated by the U.S. Government. Since research suggested that halogenated CFC emissions into the Earth's atmosphere are depleting the protective ozone layer, the international community through the Montreal Protocol has agreed to eliminate production of fully halogenated CFC's by the year 1996.

This agreement will require the air-conditioning and refrigeration industry to make rapid adjustments in design and technology to comply with the newly agreed upon standards since CFC's and HCFC's were the most common working fluids for vapor-compression cycle systems used for refrigerators well as air-conditioners for buildings and automobiles. New problems presently facing these industries include the development of new, ozone-safe refrigerants, design of new products to make use of these new refrigerants, and the retrofitting of existing products.

Since the enactment of appliance energy efficiency standards by the U.S. Government, industry has been faced with the challenge of greatly improving the energy efficiencies of their products. If industry were to obtain a better understanding of the physical and thermodynamic behavior of the new refrigerants being developed, companies would be more likely to successfully at achieve the mandates that the federal government has laid out for them. Also, that knowledge would put those companies well positioned to face inevitable stricter energy standards in the future.

The goal of this paper is to present heat transfer and pressure drop data during the condensation of the recently developed refrigerant, Genetron AZ-20, and to examine various methods for taking into account ester oil mixing effects. AZ-20 is a newly developed refrigerant, which is an azeotropic mixture of 50% HFC-32 (Pentafluoroethane) and 50% HFC-125 (Difluoromethane). Research of R-32/125 mixture is important since it is an ozone-safe replacement for HFC-22, and the properties of each refrigerant differ from each other. The experiments described within this thesis examine condensation within a smooth, horizontal tube for both the pure refrigerant and oil-refrigerant mixtures with three different oil concentrations.

The presentation of these results will hopefully provide some insight as to the characteristics of the new refrigerant as well as provide a better understanding of two-phase flow. An understanding of the flow patterns of refrigerants as they condense and how those patterns affect the condenser's performance can aid in the design of more energy efficient heat exchangers. Also, since lubrication of the compressor in vapor-compression cycle systems requires small amounts of oil to be mixed within the refrigerant, knowing the effects of oil contamination of refrigerants at various concentrations on heat transfer and pressure drop can be very beneficial.

Chapter 2 gives a theoretical background for condensation within a smooth, circular, horizontal tube. This background is provided through a summary of past research reported in the literature on this subject. A description of two-phase flow characteristics is presented so as to give the reader a better understanding of flow patterns and the significance of flow-patterns on heat transfer performance. Methods for predicting heat transfer and pressure drop and the development of those methods are presented as well as how to incorporate oil-effects into these correlations.

Chapter 3 describes the experimental apparatus and instrumentation used to perform these experiments. A detailed explanation of how the test section was designed and built as well as how the experimental loop works are presented. Furthermore, descriptions of the data acquisition system used for this project and the instrumentation involved are provided.

Chapter 4 gives in full detail the procedure used for running all of the experiments contained herein. It is explained how this procedure is meant to simulate conditions in an actual refrigerator or air-conditioner condenser. Procedures for operating the apparatus are presented so that others may repeat these experiments if desired, or perhaps improve upon the procedures used here.

Chapter 5 describes the methods used for calculating the results of the experiment and for the data reduction. The data reduction is primarily achieved through energy balances, and an explanation of how the various heat transfer coefficients and heat loss values are found is provided.

Chapter 6 presents the results of the experiments that were conducted. Charts and graphs demonstrating relations of the heat transfer to various variables as well as comparisons of the pure refrigerant data to those of the oil-refrigerant mixtures are given. The goal of this chapter is to provide the reader with information necessary to understand the trends of these tests and to show how these results compare with previously developed correlations. In addition, a number of methods for taking into account oil contamination effects are examined. Possibilities for fitting oil-refrigerant mixtures into pure refrigerant correlations are numerous, though many researchers in the past have glossed over this subject.

Lastly, Chapter 7 provides the conclusions developed from the analysis of the results and gives recommendations for potential improvements for any further research to be conducted on this subject.

Chapter 2: Theoretical Background and Literature Review

In the past, a considerable amount of both theoretical and experimental research has been performed on condensation and two-phase flow. In this chapter, a theoretical background and a review of past research on condensation and two-phase flow is provided. First, an explanation of two-phase flow is presented which describes the various flow patterns that are encountered in the condensation of refrigerants within the ranges of the parameters investigated. Next, a discussion of the heat transfer that occurs during condensation is presented, including analyses and correlations developed by various researchers in the past. In this discussion, oil contamination and mixing rules are also discussed. Finally, a discussion of the pressure drop occurring in condensation is presented.

2.1 Two-Phase Flow

As a two-phase fluid loses heat while flowing through a tube, the flow pattern, or shape of the liquid-vapor interface, will change. A number of researchers have developed flow pattern maps to help predict the flow patterns that would be encountered for various conditions. Being able to predict the flow pattern is important since the heat transfer properties will change with differing patterns.

Various authors have devised numerous classifications for flow patterns, though they all seem to fit into similar categories. As vapor flows into the condenser, forced convection transfers heat away from the fluid, and liquid then condenses on the surface of the tube. For the case of high mass flux, high velocity flows, liquid wets the entire surface of the tube, creating an annular film. The corresponding flow pattern is called the *Annular* flow regime. In the annular flow regime heat is primarily transferred by forced convective condensation through the annular film. If the mass flux is too high, liquid droplets are entrained into the high speed vapor core, creating the *Misty* or *Spray* flow regime. As the vapor continues to condense and decelerate, the liquid gathers at the bottom of the tube, creating the *Wavy* flow regime. As the liquid content of the fluid continues to grow, the liquid will occasionally wash across the top of the tube, which characterizes the *Slug* flow regime. Finally, before the liquid becomes completely sub-cooled, the *Plug* flow regime is encountered, in which there exists mostly liquid with intermittent large bubbles of vapor. Combinations of the flow regimes are very common as the flow undergoes transition from one regime to the next.

For low mass flux conditions, annular flow may be encountered, though perhaps only briefly. Generally, for low mass flux conditions, the flow changes directly from superheated vapor to the wavy flow regime since the vapor core's shear force tends to not be strong enough to push the liquid film along the sides of the tube. As the vapor continues to condense, the flow regime changes directly from wavy flow to the plug flow regime because the vapor core does not have enough shear to wash the liquid along the top of the tube. Occasionally at very low mass fluxes [vapor Reynolds number < 35000; see Chato (1962)], the *Stratified* flow regime is encountered instead of wavy flow. The stratified flow regime is similar to the wavy flow regime, except that there are virtually no waves at the liquid-vapor interface. Diagrams showing the various flow regimes and their profiles can be seen in Figures 2.1 and 2.2.

One of the first researchers to develop maps for predicting flow regime was Baker (1958), who based a flow regime map on the following two correction factors:

$$\lambda = [(\rho_v / \rho_{air}) / (\rho_l / \rho_{water})]^{1/2} \tag{2.1}$$

$$\psi = (\sigma_{water} / \sigma)[\mu_l(\rho_{water} / \rho_l)^2]^{1/3} \quad (2.2)$$

The map that Baker developed was only valid for adiabatic flow, which would involve negligible changes in quality. Condensation, however, involves heat transfer and changes in quality. To take this into account, Soliman and Azer (1971) used a non-dimensional form of Baker's parameters and adjusted Baker's map for condensing flows as shown in Figure 2.3. The dashed lines on the map represent the range covered by Soliman and Azer's study.

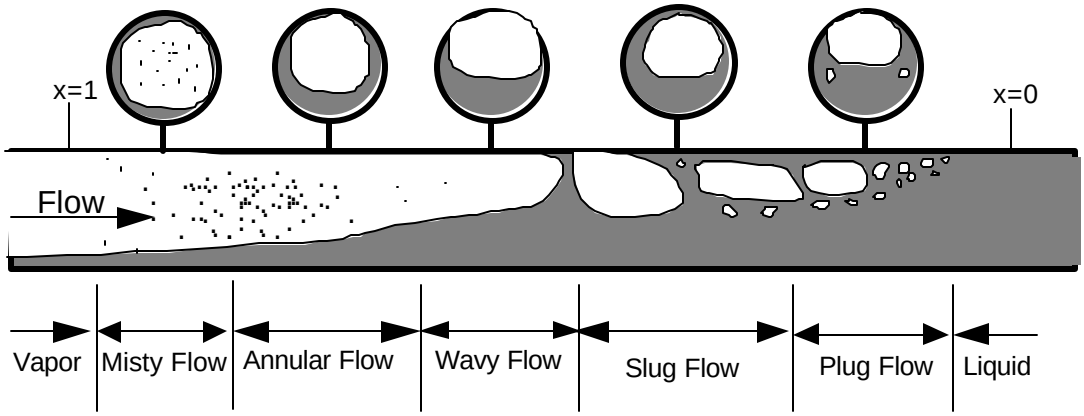

Figure 2.1 Diagram of Flow Regimes for High Mass Fluxes

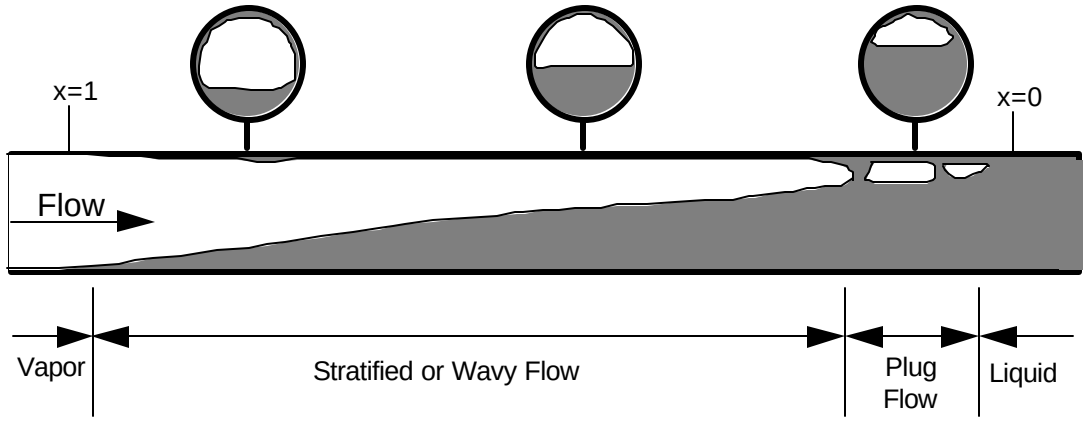

Figure 2.2 Diagram of Flow Regimes for Low Mass Fluxes

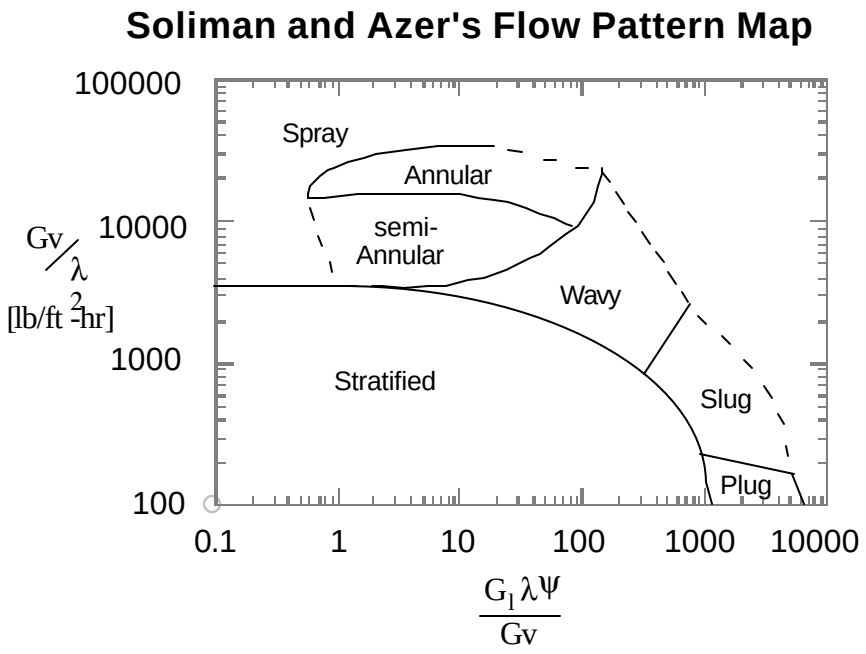

Figure 2.3 Soliman and Azer (1971) Flow Pattern Map

2.2 Development of Condensation Heat Transfer Coefficient Correlations

This section demonstrates how correlations for predicting the heat transfer coefficient of condensing flows have developed over the years. Using the Buckingham Pi theorem, it is found that the desired dimensionless groups governing boiling and condensation processes consist of ten variables in five dimensions (length, time, mass, energy, and temperature). These variables can be grouped into the following forms (Incropera and DeWitt 1990):

$$Nu_L = \frac{hL}{k} = f\left\{\frac{\rho g(\rho_L - \rho_v)L^3}{\mu^2}, \frac{C_p \Delta T}{h_{fg}}, \frac{\mu C_p}{k}, \frac{g(\rho_L - \rho_v)L^2}{\sigma}\right\} \tag{2.3}$$

or

$$Nu_L = f\left\{\frac{\rho g(\rho_L - \rho_v)L^3}{\mu^2}, Ja, Pr, Bo\right\} \tag{2.4}$$

Nusselt was the first to analyze film condensation, though his analysis was performed for a flat, vertical plate. The assumptions made in this analysis are the following:

1. The liquid film is assumed to have constant properties and laminar flow.
2. The vapor is assumed to be a pure gas at a uniform temperature equal to the saturation temperature. Since the temperature is assumed to be uniform, heat transfer only occurs at the vapor-liquid interface with no conduction occurring within the vapor.
3. The shear stress at the interface is assumed to be negligible, which allows the vapor velocity and thermal boundary layers to be ignored.

4. Momentum and energy transfer by advection in the condensate film is assumed to be negligible. This assumption is due to the low velocities of the liquid film. Heat transfer across the film is only through conduction, so the liquid temperature distribution is linear.

After solving for the liquid film thickness and applying momentum and energy equations, Nusselt derived the following equation:

$$Nu(z) = \left[\frac{\rho_l(\rho_l - \rho_v) g \sin\theta \, h_{fg} z^3}{4 \mu_l k_l (T_{sat} - T_w)} \right]^{0.25} \tag{2.5}$$

Rohsenow (1956) suggests that advection effects ican be included by using a modified latent heat of vaporization:

$$h'_{fg} = h_{fg} + 0.68 C_{P,l}(T_{sat} - T_w) = h_{fg}(1 + 0.68Ja) \tag{2.6}$$

The analysis of Nusselt (Incropera and DeWitt 1990) was extended to condensation on the outer surface of a horizontal tube, and the average convection coefficient is found to be:

$$\bar{h}_D = 0.729 \left[\frac{\rho_l(\rho_l - \rho_v) g \, k_l^3 \, h'_{fg}}{\mu_l (T_{sat} - T_w) D} \right]^{0.25} \tag{2.7}$$

For condensation inside horizontal tubes, conditions within the tube strongly depend on the vapor velocity. For low vapor velocities, the condensing liquid film is laminar and will behave similar to condensation on the outside of a horizontal tube. However, the outside tube analogy will only be correct if there is negligible vapor velocity and only for the upper part of the tube which is not covered by the thick later of liquid flowing axially at the bottom of the tube. Therefore, Chato (1962) recommends the application of a correction factor of 0.77 to the Nusselt derivation, which becomes

$$\bar{h}_D = 0.555 \left[\frac{\rho_l(\rho_l - \rho_v) g \, k_l^3 \, h'_{fg}}{\mu_l (T_{sat} - T_w) D} \right]^{0.25} \tag{2.8}$$

where

$$h'_{fg} = h_{fg} + \frac{3}{8} C_{P,l}(T_{sat} - T_w) \tag{2.9}$$

and

$$Re_{v,i} < 35000, \text{ where } Re_{v,i} = \frac{GDx}{\mu_v}.$$

At higher mass fluxes vapor shear forces will cause the laminar condensate film to become turbulent and will reduce the depth of the condensate flowing axially at the bottom. Many analyses have been performed to examine turbulent condensation with vapor shear, but most fall into one of two categories. Either the Martinelli analogy is used, in which film velocity is solved by assuming universal velocity correlations from single phase data; or the Deissler approach is used, in which the eddy diffusivity of heat and momentum, ε_h and ε_m, are predicted from single phase data. Regardless of which method is used, the following equations from Prandtl are used:

$$\frac{q}{\rho_l C_{P,l}} = -(\alpha + \varepsilon_h)\frac{dT}{dy} \tag{2.10}$$

$$\frac{\tau}{\rho_l} = (\nu + \varepsilon_m)\frac{du}{dy} \tag{2.11}$$

These two equations are used to solve for the heat flux and shear stress of the liquid, where α represents the thermal diffusivity.

In this thesis, a number of correlations are compared, all of which have been tested experimentally with refrigerants at similar conditions to the experiments performed for this project. The first turbulent film correlation that is examined is the Traviss correlation (Traviss, et al. 1973), which is based on condensation experiments performed with CFC-12 and HCFC-22. Traviss uses the momentum and heat transfer analogy and applies it to an annular flow model using the Von Karman universal velocity distribution to describe the liquid film. Traviss assumes annular flow and also assumes the flat plate analogy since the film thickness is thin. Traviss uses the Lockhart-Martinelli parameter, X_{tt}, as shown below to account for two-phase frictional pressure drop. This parameter is also used in other correlations in this chapter.

$$X_{tt} = \frac{\left(\frac{dP}{dz}\right)_l}{\left(\frac{dP}{dz}\right)_v} = \left(\frac{1}{x} - 1\right)^{0.9}\left(\frac{\rho_l}{\rho_g}\right)^{0.5}\left(\frac{\mu_l}{\mu_v}\right)^{0.1} \tag{2.12}$$

The Traviss correlation is the following:

$$Nu_{TP} = \frac{h_{TP} D}{k_l} = F_1 \frac{Pr_l Re_l^{0.9}}{F_2}, \qquad 0.15 < F_1 < 15 \quad , \quad Pr_l > 3 \tag{2.13}$$

where

$$F_1 = 0.15\left(\frac{1}{X_{tt}} + 2.85\, X_{tt}^{-0.476}\right)^a \qquad Re_l = \frac{GD(1-x)}{\mu_l} \tag{2.14}$$

a=1 for $X_{tt} > 0.155$

a=1.15 for $X_{tt} < 0.155$

$F_2 = 0.707\ Pr_l Re_l^{0.5}$ for $Re_l < 50$

$F_2 = 5\ Pr_l + 5\ \ln\left[1 + Pr_l\left(0.0964\ Re_l^{0.585} - 1\right)\right]$ for $50 < Re_l < 1125$

$F_2 = 5\ Pr_l + 5\ \ln(1 + 5\ Pr_l) + 2.5 \ln\left(0.00313\ Re_l^{0.812}\right)$ for $Re_l > 1125$

The results of this correlation tend to underestimate the misty flow regime, and Traviss attributes this increase in heat transfer to a thinner film due to entrainment of the liquid into the vapor core. Traviss claims that this entrainment occurs mostly at the entrance to the condenser.

A second correlation that is similar to Traviss' is the correlation developed by Cavallini and Zecchin (1974). The Cavallini-Zecchin correlation is a semi-empirical equation that also assumes annular flow and was tested for R-11, R-12, R-21, R-22, R-113, and R114. The Cavallini-Zecchin correlation is the following:

$$Nu = 0.05\ Re_{eq}^{0.8}\ Pr^{0.33} \tag{2.15}$$

where

$$Re_{eq} = Re_v\left(\frac{\mu_v}{\mu_l}\right)\left(\frac{\rho_l}{\rho_v}\right)^{0.5} + Re_l \qquad \text{and} \qquad Re_v = \frac{GDx}{\mu_v}.$$

This correlation predicts the experimental data of their study with a mean deviation of 30%.

The next correlation examined in this review is the one developed by Shah (1979). Shah's correlation is an empirical relation that uses the Dittus-Boelter correlation for single-phase liquid heat transfer. Shah tested the correlation for liquid Reynold's Numbers below 69000 in smooth tubes having inner diameters of 7 mm (0.277 in.) to 40 mm (1.575 in.) and for many fluids, including R-11, R-12, R-113, water, methane, ethanol, and benzene. Shah based the correlation on the observation that heat transfer processes during film condensation and during boiling without bubble nucleation are similar. The Dittus-Boelter equation used for the Shah correlation is the following:

$$h_{Lo} = 0.023\left(\frac{GD}{\mu_l}\right)^{0.8} Pr_l^{0.4}\frac{k_l}{D} \tag{2.16}$$

Shah theorized that in the process of condensation liquid forms whenever vapor contacts the pipe surface, so the circumference of the pipe is wetted at all points at all flow rates at all orientations. Shah's concluding equation is the following:

$$h_{TP} = h_{Lo}\left[(1-x)^{0.8} + 3.8\frac{x^{0.76}(1-x)^{0.04}}{P_r^{0.38}}\right] \tag{2.17}$$

Shah's correlation is good for liquid Reynolds numbers from 100 to 63000 and liquid Prandtl numbers from 1 to 13, and the mean deviation of Shah's data is 15-17%.

An empirical correlation developed by Chen et al. (1987) for shear dominated flow in vertical tubes can also be used for horizontal tubes and is as follows:

$$Nu = 0.036A^{0.50}\ Pr_l^{0.65}\ Re_l^{0.20}\left(Re_{lo} - Re_l\right)^{0.70} \qquad 40 < Re_{lo} < 18000 \tag{2.18}$$

where

$$A = 0.252\left(\frac{\mu_g}{\mu_l}\right)^{0.156}\left(\frac{\rho_l}{\rho_g}\right)^{0.78} \qquad Re_l = \frac{GD(1-x)}{\mu_l}$$

$$Re_{lo} = \frac{GD}{\mu_l}.$$

Chen compares his correlation to experimental data found in work presented by past researchers and it accurately predicts the average heat transfer coefficient, though only for the annular flow regime.

The last pure refrigerant correlation examined here was developed by Dobson et al. (1994) and consists of two correlations, one correlation for the wavy flow regime and a second one for the annular flow regime. The wavy flow correlation uses forced convective and filmwise condensation components. The test conditions used to develop the correlation included a mass flux range of 75-500 kg/m^2-s (55,000-365,000 lb$_m$/ft^2-hr) and saturation temperatures of 35 and 60 °C (95 and 140 °F).The correlation was extensively tested for 0.1875, 0.250, and 0.375 in. (3.14, 4.57, and 7.04 mm) o.d. tubes using the refrigerants R-134a, R-22, 50/50 R-32/125, and 60/40 R-32/125 and is the following:

$$Nu = \frac{0.23\,Re_{vo}^{0.12}}{1+1.11\cdot X_{tt}^{0.58}}\left[\frac{Ga\cdot Pr}{Ja}\right]^{0.25} + (1-\theta_1/\pi)Nu_{forced} \tag{2.19}$$

where

$$1-\frac{\theta_1}{\pi} \cong \frac{\arccos(2\alpha-1)}{\pi} \tag{2.20}$$

$$Nu_{forced} = 0.0195\,Re_l^{0.8}\,Pr_l^{0.4}\,\phi_l(X_{tt})$$

$$\phi_l(X_{tt}) = \sqrt{1.376+\frac{c_1}{X_{tt}^{c_2}}}$$

The symbol, θ_1, represents the angle from the bottom of the tube to the point where the liquid level meets the tube wall. The function $\phi_l(X_{tt})$ represents the two-phase multiplier developed by Souza (1993) and the constants, c_1 and c_2, are determined from the liquid Froude number as follows:

$$c_1 = 4.172 + 5.48Fr_l - 1.564Fr_l^2 \qquad \text{For } 0 < Fr_l \le 0.7$$
$$c_2 = 1.773 - 0.169Fr_l$$

and

$$c_1 = 7.242 \qquad \text{For } Fr_l > 0.7$$
$$c_2 = 1.655$$

The annular flow correlation resembles the Shah correlation in that a regression analysis of annular flow data was used with the Dittus-Boelter single-phase correlation, and is shown below:

$$Nu = 0.023\,Re_L^{0.80}\,Pr_l^{0.4}\,g(X_{tt}) \tag{2.21}$$

where

$$g(X_{tt}) = 1+\frac{2.22}{X_{tt}^{0.889}}. \tag{2.21a}$$

The criteria used for determining whether to use equation (2.19) or equation (2.21) is the following:

1) If the mass flux is less than 364 klb/ft^2-hr (500 kg/m^2-s), equation (2.19) should be used for Fr_{so} < 20 and equation (2.21) should be used for Fr_{so} >20.
2) If the mass flux is equal to or greater than 364 klb/ft^2-hr (500 kg/m^2-s) equation (6.21) should be used.

Fr_{so} is the Solimann Froude number and is the following:

$$Fr_{SO} = 0.025 Re_l^{1.59} \left(\frac{1 + 1.09 X_{tt}^{0.039}}{X_{tt}} \right) \frac{1}{Ga^{0.5}} \qquad \text{for } Re_l \leq 1250$$

$$Fr_{SO} = 1.26 Re_l^{1.04} \left(\frac{1 + 1.09 X_{tt}^{0.039}}{X_{tt}} \right) \frac{1}{Ga^{0.5}} \qquad \text{for } Re_l \leq 1250 \tag{2.22}$$

The Dobson correlation accurately predicted the experimental data for average qualities of 10-90% with a mean deviation of 4.5%.

2.3 Pressure Drop Correlations

For horizontal condensation the pressure drop consists of two components, pressure drop due to friction and pressure drop due to momentum change, and is described by the following equation:

$$\left(\frac{dP}{dz} \right) = \left(\frac{dP}{dz} \right)_f + \left(\frac{dP}{dz} \right)_m \tag{2.23}$$

Inside a typical horizontal condenser the momentum pressure drop is generally much smaller than the frictional pressure drop so emphasis is put primarily on the prediction of the friction pressure gradient. The pressure drop is commonly predicted using a two-phase friction multiplier, ϕ^2, and three equivalent expressions for the pressure gradient due to friction are presented as demonstrated by Schlager et al. (1990):

$$\left(\frac{dP}{dz} \right)_f = \left(\frac{dP}{dz} \right)_{fl} \cdot \phi_l^{\,2} = -\frac{2 f_l G^2 (1-x)^2 v_l}{D} \cdot \phi_l^{\,2}$$

$$\left(\frac{dP}{dz} \right)_f = \left(\frac{dP}{dz} \right)_{flo} \cdot \phi_{lo}^{\,2} = -\frac{2 f_{lo} G^2 v_l}{D} \cdot \phi_{lo}^{\,2}$$

$$\left(\frac{dP}{dz} \right)_f = \left(\frac{dP}{dz} \right)_{fv} \cdot \phi_v^{\,2} = -\frac{2 f_v G^2 x^2 v_v}{D} \cdot \phi_v^{\,2} \tag{2.24}$$

where the friction factor, f, is calculated by turbulent flow calculations such as

$$f = \frac{0.079}{Re^{0.25}} \quad \text{or} \quad f = \frac{0.046}{Re^{0.2}} \tag{2.25}$$

and where the subscripts 'l', 'lo', and 'v' represent the models of the flow being based on liquid properties, based on assuming the flow is all liquid, and based on vapor properties, respectively. The corresponding Reynolds numbers are the following:

$$Re_l = \frac{GD(1-x)}{\mu_l}$$

$$Re_{lo} = \frac{GD}{\mu_l}$$

$$Re_v = \frac{GDx}{\mu_l} \tag{2.26}$$

Generally, pressure drop correlations fall under the classification of the homogenous model or as a separated flow model. The homogenous model assumes that the vapor and liquid velocities are the same. The two-phase friction multiplier for the homogenous model is

$$\phi^2_{lo} = \left[1 + x\left(\frac{v_v - v_l}{v_l}\right)\right] \cdot \left[1 + x\left(\frac{\mu_l - \mu_v}{\mu_v}\right)\right]^{-0.25} . \tag{2.27}$$

For separated flow models a generalized Lockhart-Martinelli parameter is used:

$$X^2 = \frac{\left(\frac{dP}{dz}\right)_l}{\left(\frac{dP}{dz}\right)_v} = \frac{Re_v{}^m}{Re_l{}^n} \cdot \frac{C_l}{C_v} \cdot \left(\frac{\mu_l}{\mu_v}\right)^a \left(\frac{\rho_v}{\rho_l}\right)^b \tag{2.28}$$

The Lockhart-Martinelli parameter for the condensation examined in this paper generally equals X_{tt}, which stands for turbulence in both the liquid and vapor phases and is equivalent to equation (2.12). Chisholm (1963) attempted to correlate the two-phase multiplier such that it accounted for the influence of mass flux and used the following relation:

$$\phi_l{}^2 = 1 + \frac{C}{X} + \frac{1}{X^2}$$

$$C = \left[0.75 + \left(\frac{2000}{G} - 0.75\right) \cdot \left(\frac{v_v - v_l}{v_l}\right)^{0.5}\right] \cdot \left[\left(\frac{v_v}{v_l}\right)^{0.5} + \left(\frac{v_l}{v_v}\right)^{0.5}\right] \tag{2.29}$$

where C is a dimensionless parameter. Most of the older pressure drop correlations were developed from experiments using steam as the working fluid. Souza et al. (1993) developed a correlation using data from R-12 and R-134a as the test fluids. Souza used a Froude number to take into account the flow regime, and his correlation for the two-phase multiplier is the $\phi_l(X_{tt})$ shown previously in equation (2.20).

2.4 Accounting for Oil Contamination

Many difficulties are encountered when trying to account for oil contamination during condensation. It is necessary to have oil mixed with the refrigerant in order to have lubrication of the compressor, and only a few methods have been developed to account for oil-refrigerant mixtures in correlations. One method used by Baustian et al. (1986) is to use mixture correlations for the thermodynamic properties and substitute these into pure refrigerant

correlations. A second method used by Tichy et al. (1985) is to apply a correction factor to previous pure refrigerant correlations.

For the first method, an equation for the density of oil-refrigerant mixtures is published by ASHRAE in the 1984 Handbook:

$$\rho_m = \frac{\rho_r}{1-(1-\omega)\left(1-\frac{\rho_r}{\rho_o}\right)} \tag{2.30}$$

where ω represents the mass fraction of the refrigerant. Reid et al. (1987) provided a number of methods for calculating the properties of mixtures, though these methods are not specifically for oil-refrigerant mixtures. For the linear method, the properties are calculated in the following way:

$$\begin{aligned} C_{Plm} &= x_m C_{Pl_1} + (1-x_m) C_{Pl_2} \\ k_{lm} &= x_m k_{l_1} + (1-x_m) k_{l_2} \\ \mu_{lm} &= x_m \mu_{l_1} + (1-x_m) \mu_{l_2} \end{aligned} \tag{2.31}$$

This method works well for the specific heat, C_p, but not for many of the other properties. For *ideal* mixing, it is assumed that there are no mixing effects that enhance or reduce the properties. It also assumes that the pure components have similar vapor pressures and come from similar chemical families, which certainly would not hold for oil-refrigerant mixtures. Reid suggested the following equations for the thermal conductivity and viscosity of *non-ideal* mixtures, which takes into account mixing effects.

$$\begin{aligned} k_{lm} &= x_m k_{l_1} + (1-x_m) k_{l_2} - 0.72 x_m (1-x_m) \left| k_{l_1} - k_{l_2} \right| \\ \mu_{lm} &= \exp\left[x_m \ln(\mu_{l_1}) + (1-x_m) \ln(\mu_{l_2}) \right] \\ &\quad + 0.85 \left\{ \rho_{lm} \exp\left[\frac{x_m}{\rho_{l_1}} + \frac{(1-x_m)}{\rho_{l_2}} \right] - 1 \right\} - 0.085 \end{aligned} \tag{2.32}$$

Baustian (1986) used the linear method for the specific heat and the non-ideal method for the thermal conductivity, but used the following equations for viscosity and surface tension of oil-refrigerant mixtures:

$$\begin{aligned} \mu_m^{1/3} &= x_r \mu_r^{1/3} + x_o \mu_o^{1/3} \\ \sigma_m &= \sigma_r + (\sigma_o - \sigma_r)\sqrt{1-\omega} \end{aligned} \tag{2.33}$$

Eckels and Pate (1991) used the first method by assuming that the saturation temperature is negligibly affected by the addition of oil for qualities less than 85%, which is questionable since oil concentrations of more than 1% can cause an apparent superheat of 1° F or greater (Hinde et al. 1993). Apparent superheat due to oil is discussed further in Chapter 5. Eckels and Pate found that the addition of oil lubricant decreased the condensation heat transfer coefficient and increased the pressure drop for the refrigerant HFC-134a by as much as 40%. Oil concentrations of 0 to 5.3% were tested for both CFC-12 and HFC-134a.

The second method of accounting for oil in the refrigerant requires some form of a correction or enhancement factor applied to already existing correlations. Tichy et al. (1985) used this approach with the Shah correlation (equation (2.17)) to find the following:

$$h = h_{Shah}\left[0.88 + \left(\frac{3650}{Re_l}\right)^{1.99}\right] \cdot e^{-5.0\omega_o}$$

$$Re_l = \frac{GD}{\mu_l} \tag{2.34}$$

Schlager et al. (1990) have a similar relationship developed from experimental data of R-22 and 150-SUS oil mixtures, and the correction factor they developed is the following:

$$EF_{s'/s} = \exp(-3.2 \cdot \omega_o) \tag{2.35}$$

A recent correlation to take into account oil contamination was developed by Cawte (1992), the analysis ignores the oil component of the flow and then uses a multiplier as shown below:

$$h = h_l\left\{1 + b_1\left[\left(\frac{1}{x} - 1\right)^{0.8} P_r^{\,0.4}\right]^{b_2}\right\} \tag{2.36}$$

where

$$b_1 = 5.37 + 1.85e^{-110\omega_o}$$

$$b_2 = -0.642 - 0.172e^{-65.5\omega_o}$$

$$h_l = 0.023\frac{k_l}{D} Re_l^{\,0.8} Pr_l^{\,0.4} \tag{2.37}$$

In regards to the effect of oil contamination on pressure drop, very few researchers mention correlations to take the oil into account. Of the few investigations found, most of these were inconsistent and without a theoretical basis. For instance, Tichy (1985) devised the following:

$$\Delta P = \Delta P_{corr}(0.828 + \omega_o) \tag{2.38}$$

which implies that the magnitude of the pressure drop is lower for small oil concentrations, though most experimental research demonstrates a rise in pressure drop with oil-refrigerant mixtures. It should be noted that the correlation consistently underpredicts the experimental data.

A more recent correlation to account for oil effects on pressure drop was developed by Souza et al. (1993) using a regression analysis on 157 experimental data points and is expressed as follows:

$$\Delta P_{oil} = \Delta P_{pure}(1 + 12.4\ \omega_o - 110.8\ \omega_o^{\,2}) \qquad \text{for } \omega_o < 0.056 \tag{2.39}$$

This correlation accurately predicts pressure drop for R-134a and R-12 to within ±7.5%.

Chapter 3: Experimental Apparatus and Instrumentation

This section describes the apparatus used to acquire the heat transfer and pressure drop data of the various refrigerants and refrigerant mixtures. The apparatus was used previously by Bonhomme (1991) and Hinde (1993), and the reader is urged to read their descriptions for a more in depth understanding of the initial design and data acquisition devices used in the past since emphasis in this paper is put on recent modifications and additions to the test apparatus.

3.1 Test Apparatus

The apparatus used in this investigation consists of an after-condenser, a filter-drier, a variable speed refrigerant pump, a refrigerant heater, sight glasses, an adiabatic 0.277 in. (7.0 mm) i.d. test section, a diabatic 0.277 in. (7.0 mm) i.d. test section, two refrigerant flow meters, a receiver, a water-cooled heat exchanger, a water flow meter, and a waste pump. The system, as a whole, involved a closed loop of refrigerant and an open loop of water used to condense the heated refrigerant. Most of the refrigerant loop consists of 1/2 in. o.d. copper tubing and is designed to withstand pressures up to 500 psi (3450 kPa) and temperatures up to 180 °F (82 °C). The entire loop is covered with at least 2 in. of Armaflex insulation to minimize heat loss to the environment. A schematic drawing of the refrigerant loop is shown in Figure 3.1.

Before the refrigerant is allowed to reach the variable speed pump, it must be fully condensed into a single-phase liquid, otherwise the positive displacement pump cannot effectively pump the refrigerant forward. Therefore, a water-cooled after condenser with a cooling capacity of approximately 2 tons (7.0 kW) is placed in between the test section and the receiver to subcool the fluid. The receiver is immersed in a temperature contolled water bath, which is adjusted as necessary with the receiver input control valve to control the pressure of the system.

The refrigerant then exits through the bottom of the receiver into a water-cooled, counter-flow heat exchanger, which further subcools the refrigerant before it enters the variable speed pump. A filter-drier is placed just after the heat exchanger to remove any water or dust particles to protect the system. After the refrigerant passes through the filter drier it goes through the variable speed refrigerant pump. This pump is a MicroPump three-gear, variable speed positive displacement pump with a capacity of 0.77 gpm (2.9 l/min). The pump is magnetically driven by a 1/3 hp, 3450 rpm (max) motor. There is also a valved bypass around the pump to serve as a control of refrigerant flow through the system. This provides a method of regulating the refrigerant flow that is more stable when dealing with large adjustments in the flow rate, particularly at low flow rates.

After the refrigerant travels through the pump, it passes through one of two flowmeters, depending on the magnitude of the flow rate. One is a Max 0-2 gpm (0-7.6 l/min) positive displacement flowmeter and the other is a Micro Motion 0-1 lb/min (0-0.45 kg/min) mass flowmeter. The former is used for the higher flow rates tested and the latter is used for the lower ones tested.

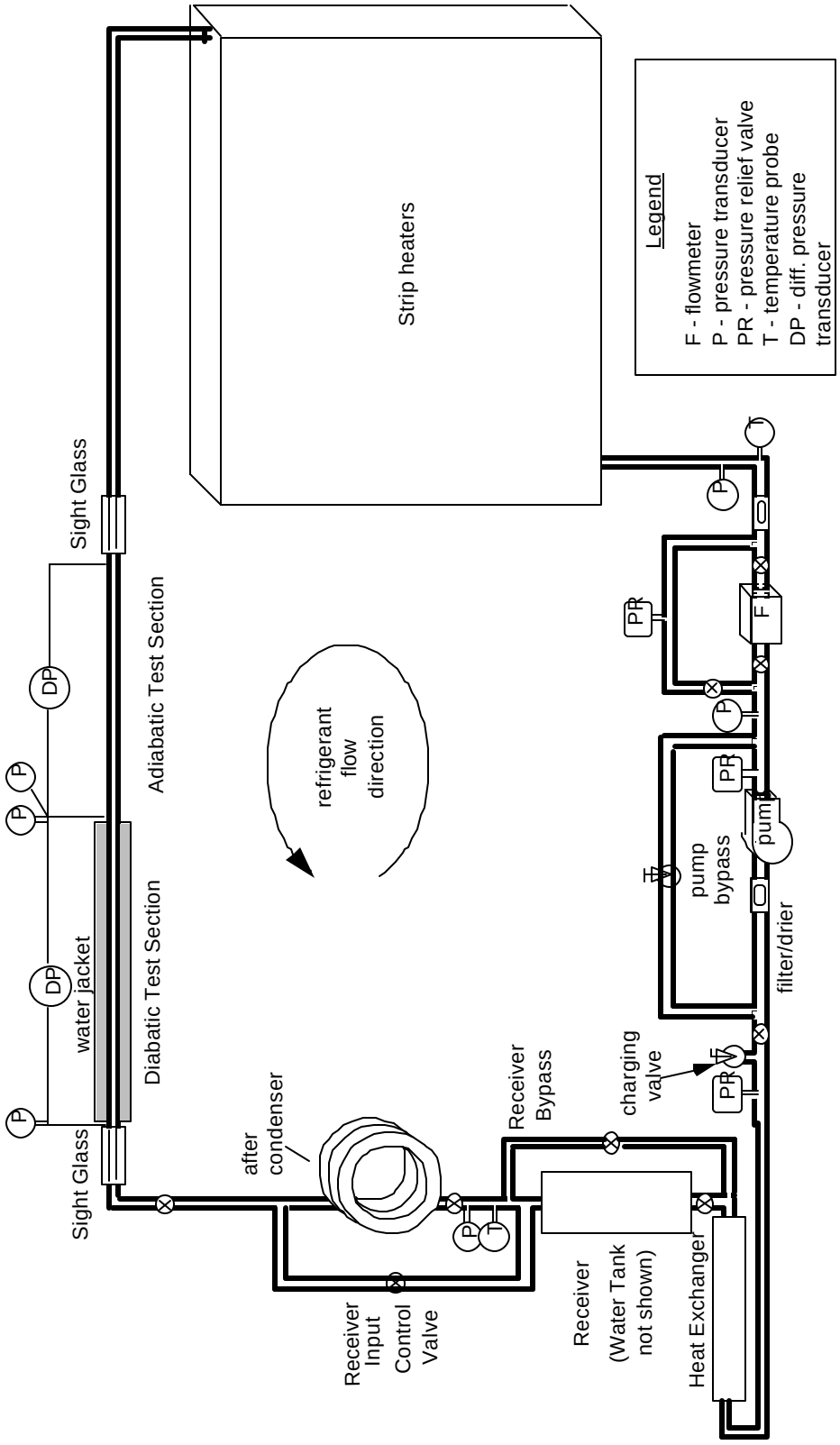

Figure 3.1 Schematic of Single Tube Condensation Test Loop

Following the flowmeters is the heater section of the apparatus. The heater consists of five passes of 3/8 in. OD copper tubing, with each pass wrapped with resistance heater tape. The heater contains four heater tapes on each pass, with each heater tape having a resistance of 180 ? , thus providing a maximum of 320 W each and delivering a maximum total of 6.4 kW. All twenty heaters can be individually turned on or off as needed for each particular experiment, and half of them are controlled by a 0-240 V Variac. Each pass, as well as the entire heater box, is thoroughly insulated with Armaflex insulation. The pass leading to the test section is kept at the same level as the test section itself to prevent the occurrence of thermosyphon effects. A schematic of the heater is shown in Figure 3.2:

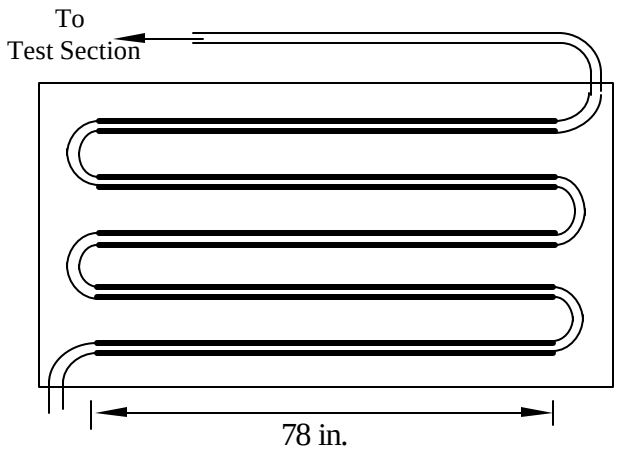

Figure 3.2 Schematic of the Heater

There are sight-glasses placed at the inlet and at the outlet of the test section so as to observe the various flow patterns of the condensing refrigerant. Each sight-glass consists of a 5 in. long glass tube with an outer diameter of 1/2 in. (12 mm) and an inner diameter of 0.277 in. (7 mm) to match the inner diameter of the test section. The tubes are connected on both sides to the copper tubes by brass Gyrolock compression tube fittings, which have all of the brass ferrules that would connect with the glass tube replaced with Teflon ferrules. The glass tubes have been annealed and are rated to withstand 500 psi (3440 kPa) of pressure. To confirm this rating, pressure tests of the sight glasses up to 500 psi (3440 kPa) are performed in a large bucket of water before installing the sight glasses into the apparatus. A schematic of the sight glasses is shown in Figure 3.3:

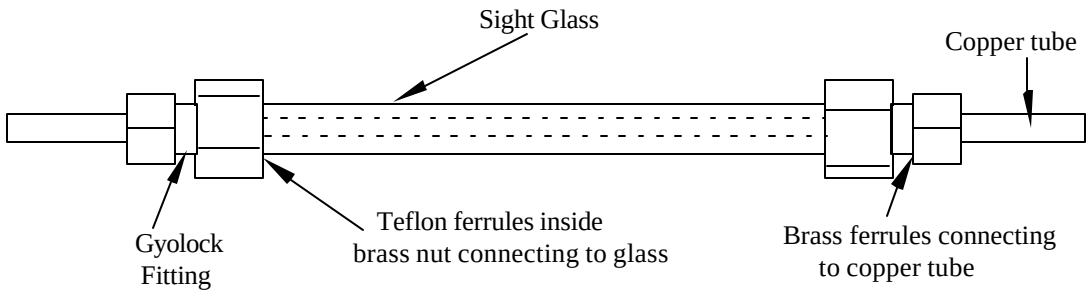

Figure 3.3 Schematic of Sight Glasses

To condense the refrigerant, a counter-flow water annulus is used, and is supplied directly from a water tap, though the water flow rate is controlled by two valves at the water inlet. One valve only controls the flow rate, and the other valve controls the water pressure, though it also affects the flow rate. Control of the water pressure is desired since air bubbles tend to form within the water at pressures less than 20 psig (137 kPa), so a simple spring pressure gauge is placed just after the control valve. The schematic of the water side of the apparatus is shown in Figure 3.4:

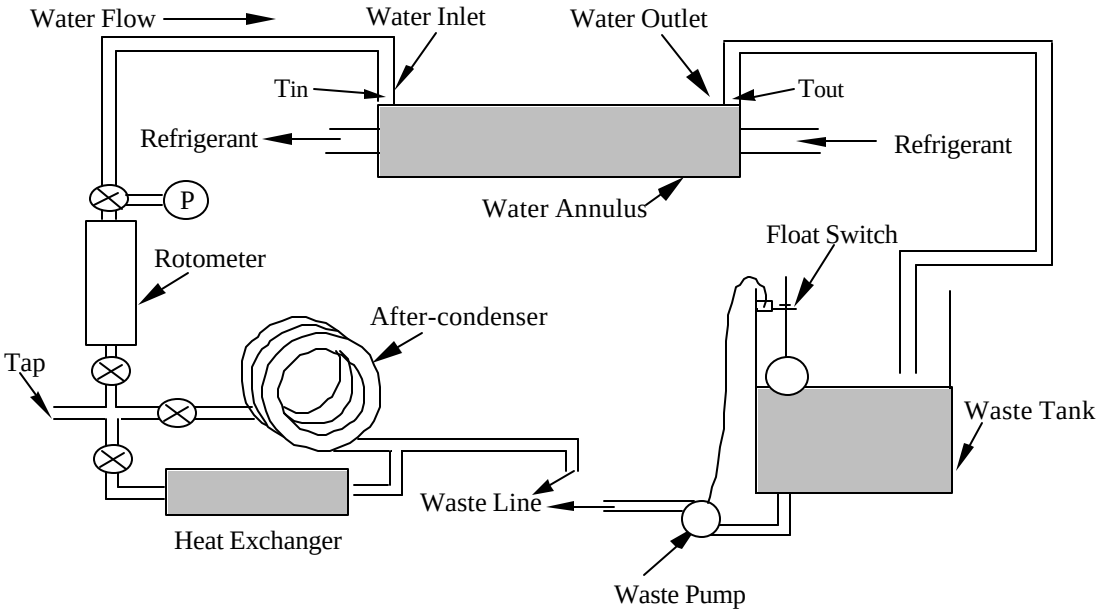

Figure 3.4 Schematic of the Water Side of the Apparatus

The rotameter is only used for a rough estimate of the water flow rate, so when taking actual test measurements a graduated cylinder and stopwatch are used for precise readings. Although it is not shown in the schematic, there is a second rotameter connected at the after-condenser's control valve, which measures 0-5 gpm (0-19 l/min). After the water flows through the after-condenser, the water flows directly into a waste line. In the case of the water exiting the test section, the water first travels from the outlet into a tube over the waste tank where the flow rate is measured manually. As the waste tank fills beyond a certain level, a float switch device starts the waste pump, which uses a single-phase 1/12 hp 1750 rpm pump motor made by the Little Giant Pump Company and pumps the water into the waste line.

The temperatures at the inlet and outlet of the water flow cooling the test section are measured to calculate the water-side heat transfer. The measurements are made using thermocouple probes with the tips of the probes oriented such that they both face into the direction of the water flow and are immersed to a length of 6-8 in. (152-203mm), which avoids errors due to fin effects. Each thermocouple is made using a Gyrolock fitting, a 1/8 in. OD brass tube, and 0.020 in. diameter Copper and Constantan thermocouple wires. The construction procedure of the probe begins with the Gyrolock fitting being fastened to the brass tube. The thermocouple wires have the insulation stripped off 1/8 in. back, and then the exposed wires are twisted together and pulled through the tube, where they are

then crimped in place with a pliers. Lastly, the entire end is filled with solder to simultaneously form a thermocouple bead and make the probe water-tight. A schematic of the thermocouple probe is shown in Figure 3.10:

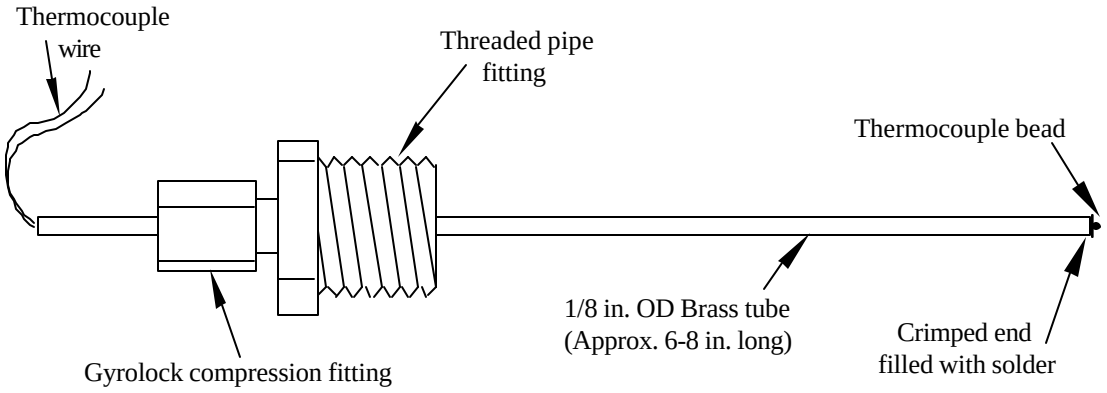

Figure 3.10 Schematic of a Water Inlet/Outlet Thermocouple

3.2 The Condenser Test Section

The test section is designed to simulate a section of a smooth, single tube condensing heat exchanger and accurately measure the heat transfer coefficients and pressure drops in condensing flows. The test section consists of two parts: one adiabatic test section used for comparing pressure drop data and one diabatic test section used for examining condensation heat transfer and pressure drop. The diabatic section uses a water annulus to cool the refrigerant. The geometry of the annulus is kept consistent by a number of spacers. The diabatic test section has five thermocouple measurement stations with four thermocouple grooves milled at each of those stations. There are also thermocouple stations just outside the inlet and outlet of the diabatic section as well as at the inlet to the adiabatic section, all of which have grooves on the top and bottom of the tube. Near each of those three stations are pressure taps, which are used for measuring both pressure drops and absolute pressures. The specifications of the test section are given in Figure 3.5:

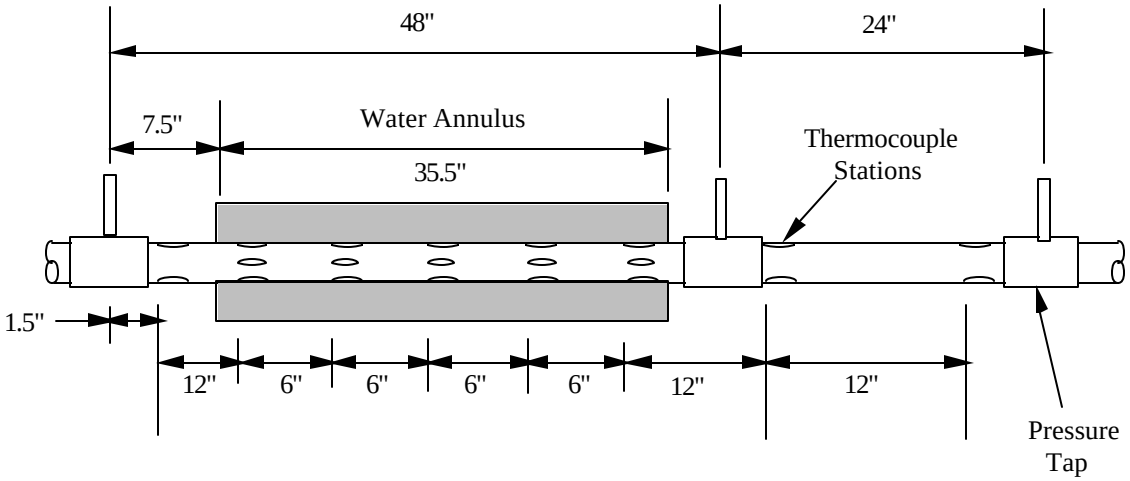

Figure 3.5 Schematic of the Test Section

The test section is constructed of copper tube and has an outer diameter of 0.375 in. (9.525 mm) and an inner diameter of 0.277 in. (7.0 mm). The water annulus is 35.5 in. (90.17 cm) long and is held in place by ten nylon washers, or spacers, which have many smaller holes drilled through the ring to allow water through and mix it as it passes. Two spacers are placed at each of the five thermocouple locations inside the annulus, with one spacer placed just upstream of the thermocouple, away from the bead, and the other spacer placed approximately 2 or 3 in. upstream of the first spacer. The spacers are shown below in Figure 3.6:

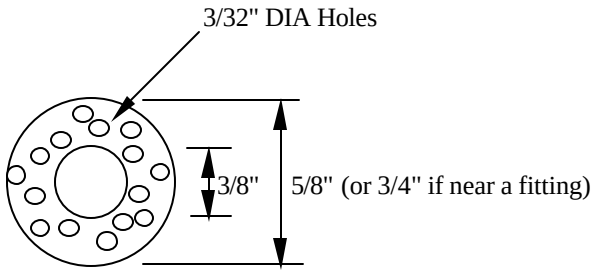

Figure 3.6 Spacer Diagram

The annulus itself is 3/4 in. (19 mm) o.d. plastic tubing and has an inner diameter of 5/8 in. (16 mm). At each thermocouple station in the annulus the thermocouple wire is drawn through a T-fitting, which is placed approximately 1 in. (2.5 mm) downstream on the water side. Since the two wires for each thermocouple are sheathed together, the sheath was stripped far enough such that the thermocouples could be glued in place to prevent the water from leaking out through capillary forces.

The thermocouples at each of the stations are positioned as shown in Figure 3.7. As can be seen, the thermocouples at the stations within the annulus are placed at 0°, 60°, 180°, and 240°. The reason for this placement is that each location represents 1/6 th of the cross-section's circumference, with the portions at 120° and 300° assumed equivalent to the portions at 240° and 60°, respectively, due to symmetry. For the thermocouple stations outside the annulus, the thermocouples are placed only at the top and bottom of the cross-section. The reason for having thermocouples outside the annulus is primarily to act as a check for inlet and outlet refrigerant temperatures of each of the test sections.

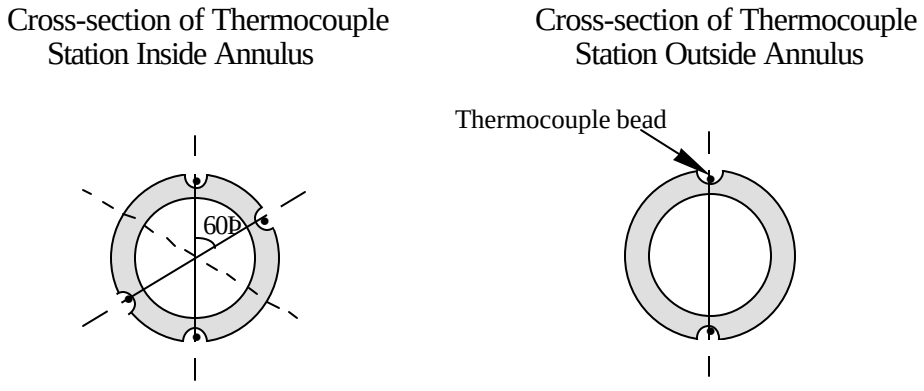

Figure 3.7 Thermocouple Positions at Each Station

The method for soldering the thermocouple wire into the grooves is provided here in detail since the temperature measurements must be as accurate as possible. First the grooves are cleaned with an alcohol-soaked Q-tip to remove residue and shavings from the milling process. Then the grooves are tinned by placing a tiny piece of fluxed solder in each groove and heating the tube with a torch. As the solder melts, it is spread around with an Exacto-knife, leaving a thin layer of solder in each of the grooves. After tinning the grooves, the Cu-wire and Cn-wire of each thermocouple are twisted together very tightly and clipped such that only about 1/8 in. of bare wire is exposed. Then the thermocouple wire is tinned with a soldering iron, and tied in place on the test section with thin wires to prevent the thermocouples from popping loose while doing the final soldering. The final soldering is done by placing a small piece of solder on the tip of the twisted thermocouple wires with some flux and then heating the tube with a propane torch. After the tube cools down, the thermocouples are sanded down to make certain that the thermocouple beads are not sticking out into the passing water flow. If the thermocouples stick out, the temperature readings may be faulty due to the thermal boundary layer and fin effects. The thermocouples are then cleaned once again with alcohol, and a thin layer of thermally conductive epoxy is placed over any exposed bare wire to fill the groove and prevent water from wicking down the thermocouple wires. A schematic of a single thermocouple groove is shown in Figure 3.8:

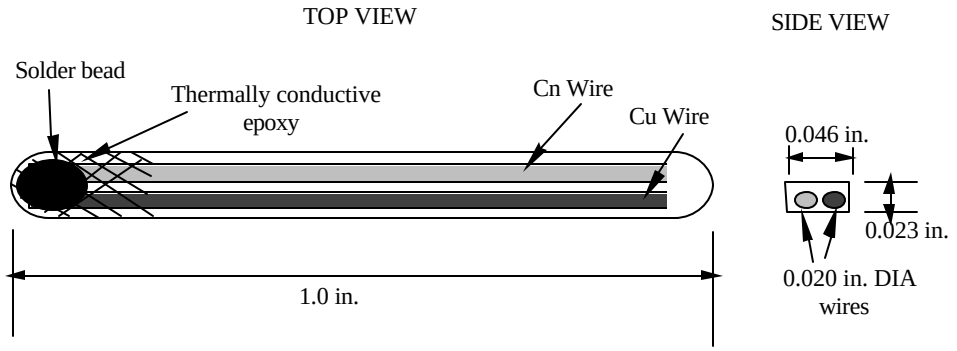

Figure 3.8 Individual Thermocouple Groove

In past test sections, such as the one used by Hinde et al. (1993), pressure taps were specially made by a machine shop. For this test section, however, it was found that the three pressure taps are relatively easy to make using tube fittings, 1/8 in. o.d. copper tubing, braze, and solder. A schematic of how each pressure tap is constructed is shown in Figure 3.9:

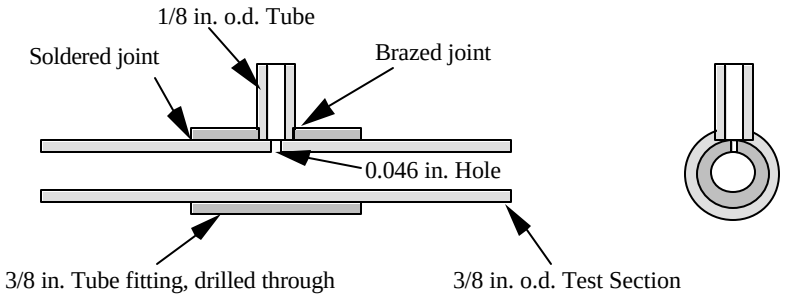

Figure 3.9 Pressure Tap Schematic

The method used to make the pressure tap was to first drill an 1/8 in. hole through a 3/8 in. i.d. copper tube fitting, and then braze a 1/8 in. o.d. tube that is approximately 7/8 in. long into that hole. The 3/8 in. fitting is then drilled through with a 3/8 in. diameter drill bit to remove the center ridge inside. The fitting is then slid down the test section to the proper position and soldered with a lower temperature solder than the braze. After the soldering is complete, a 0.046 in. hole is drilled through the 1/8 in. tube and through the test section. If the 1/8 in. tube is too long, there is a likelihood that the drill bit will break when drilling the final 0.046 in. hole. A good rule of thumb is to keep the tube less than 20 diameters or so long. To lessen the likelihood of a burr forming from the drilling, a smaller diameter drill bit of 0.042 in. is used to drill an initial hole, then the 0.046 in. drill bit is used to complete the pressure tap, and finally a cloth wrapped around a small tube is passed through the test section to break off any rough burrs that happen to stick out. The reason that such care is taken to remove burrs is that burrs may cause errors in the pressure readings. The pressure taps are connected to the pressure transducers through either solder fittings or through Gyrolock fittings.

The order in which each component of the test section is constructed is crucial. The reason is that if one component is soldered in first, it may make it impossible to add a second component in the desired position. The order in which the apparatus is constructed is as follows:

1. Slide each of the thermocouple fittings and annulus over the test section.
2. Slide all of the thermocouples for a particular station through the necessary fittings and solder the thermocouples into the grooves.
3. Repeat 2. for each successive thermocouple station.
4. Glue spacers at the proper positions.
5. Glue the fittings and annulus in place
6. Solder and drill pressure taps in place.
7. Solder in the surface thermocouples that are outside of the water annulus.
8. Block the exit areas of the thermocouple wires with glue.

3.3 Instrumentation and Data Acquisition

The instrumentation used in this study includes thermocouples, power transducers, mass and volumetric flowmeters, absolute pressure transducers, and differential pressure transducers. All of the above instruments relay signals to the data acquisition equipment, which then sends the information to a computer for both on-line and off-line analysis.

Two different brands of thermocouple wires are used in this apparatus, one of which is only used for the thermocouple probes and the other is used for surface temperature readings. The thermocouples used in the probes are 30 gauge Copper-Constantan, type-T Omega thermocouples. The probes are placed at the refrigerant heater inlet, the inlet and outlet of the refrigerant side of the test section, the inlet and outlet of the water side of the test section, and the inlet and outlet of the aftercondenser. The surface thermocouples used are also 30 gauge Copper-Constantan type-T, though these wires are made by Multi-Cable Corporation and the wires are sheathed together in Teflon insulation. It should be noted here that the insulation must be peeled back from the tip to just past where glue is holding the wires in place. The reason for this is to prevent water from wicking up through the sheath, which could

prove hazardous to the data acquisition boards. Both brands of the thermocouples are calibrated from 32-76 °F (0-80 °C) using a constant temperature bath and precision Mercury thermometers. The thermocouples are specified as having accuracies of ±0.18 °F (±0.1 °C).

The power transducers used to measure heat input to the refrigerant heaters and the flow meters used to measure the mass flux of the refrigerant are identical to the instruments used by Hinde et al. (1993). The power transducers consist of two Ohio Semitronics Watt-hour transducers that measure heat input in steps of 100 mW, with an accuracy rating of ±0.2%. The mass flowmeter is a Micro Motion 0-1 lb/min (0-0.45kg/min) flowmeter with a 2-10 V output signal and is rated at ±0.1% of full scale output. The volumetric flowmeter is a Max Machinery 0-2 gpm (0-7.6 l/min) positive displacement flowmeter with a 0-10 V output signal and is rated at ±0.31% of full scale output.

Absolute pressure readings are measured at the heater inlet, the test section inlet and outlet, and at the aftercondenser inlet and outlet. All transducers are calibrated using a dead weight tester. The transducers used at the heater inlet, the test section outlet, and at the aftercondenser are all Setra 0-1000 psia (0-6900 kPa) pressure transducers with accuracy ratings of ±0.11%. All of the above transducers have an output of 0-5 V. At the test section inlet there are two pressure transducers, both of which are manufactured by BEC Controls Corporation. One of the transducers is 0-500 psia (0-3400 kPa) with an output of 0-5 V and an accuracy rating of ±0.1%. The other transducer is 0-300 psia (0-2070 kPa) with an output of 2-10 V, and also has an accuracy rating of ±0.1%. Differential pressure measurements to measure pressure drop across the test section are made using two Sensotec ±0-5 psid (0-33 kPa) differential pressure transducers with 0-5 V outputs and ratings of ±0.25% of full scale.

The data acquisition is accomplished using an Apple Mac IIci computer in conjunction with a data acquisition board from National Instruments, which is a NB-MIO-16L multifunction I/O board installed in a Nubus card slot within the computer, and a Campbell Scientific 21X Datalogger, which sends data to the computer from two 24-channel Campbell Scientific AM64 multiplexers through the serial port. The computer then processes the data on-line using National Instruments' Lab View 2.2 data acquisition software, which displays select data on the computer screen to aid in the monitoring of experiments being performed. The software also allows data to be saved to a file when desired, and the data are later processed off-line using Excel 4.0.

Chapter 4: Experimental Design and Procedure

In this chapter, the experimental design and procedure for this study is discussed. First, an explanation of what the study was designed to simulate is provided, and then the actual test conditions of the experiments used for this study are described. A discussion of the experimental procedure is presented, as well as the methods used for injecting the oil lubricant into the system and how to measure the oil concentration of the resulting oil-refrigerant mixture.

4.1 Simulation Conditions

The test apparatus was built with the intention of simulating various conditions found in typical domestic refrigerators, household and automobile air conditioners. These conditions can be identified through the following parameters: mass flux, saturation temperature, vapor quality, and oil concentration. Typical refrigerant mass flow rates found in the above appliances can range from as low as 10 lb_m/hr (4.5 kg/hr) in domestic refrigerators to as high as 900 lb_m/hr (410 kg/hr) in automobile air conditioners. In a 0.277 in. ID (7 mm) tube these flow rates would have a mass flux range of 24,200-2,200,000 lb_m/ft^2-hr (33-3000 kg/m^2-s). For this study, the mass fluxes examined tend to fall in the lower and middle areas of that range. Typical saturation temperatures for domestic refrigerators have a range of 90-140 °F (32-60 °C). The saturation temperature at which all of the tests were performed was approximately 95 °F (35 °C), which is in the lower portion of that range. Typical oil concentrations range from 1-5%, and all oil-refrigerant mixture experiments in this study lie within this concentration range.

4.2 Test Conditions

The tests performed in this study include the condensation of pure R-32/125 and the condensation of mixtures of R-32/125 with three different concentrations of an ester oil lubricant for use with refrigerants. The lubricant used was developed by ICI Chemicals & Polymers, Ltd. and its trade name is Emkarate RL 184. These tests were performed in a 0.277 in. ID smooth copper tube as described in Chapter 3. The test conditions consisted of mass fluxes of 55000, 110000, 220000, and 364000 lb_m/ft^2-hr (75, 150, 300, and 500 kg/m^2-s) at 95 °F (35 °C), with average qualities ranging from 0.10-0.90. For consistency, the difference between the test section average saturation temperature and average wall temperature was kept constant at approximately 5.4 °F (3 °C). All of the test conditions are summarized in Table 4.1.

4.3 Experimental Procedure

The methods used for running the tests in this study were fairly different from those used by Bonhomme (1989) and Hinde (1993). The major differences mostly come from the change in the way that the saturation pressure was controlled and in the way that oil concentrations were measured. In place of the bladder-accumulator setup, which used nitrogen to control the system pressure, a receiver immersed in a temperature controlled water bath was used for this study. For the case of oil concentration measurements, a gas chromatograph analyzer was used since the supply of R-32/125 was limited, which makes the ASHRAE Standard 41.4 impractical to use.

Test Fluid	Average Concentration of Oil	Mass Flux	Saturation Temperature and Quality
Pure R-32/125	0%	55,000 lbm/ft^2-hr (75 kg/m^2-sec)	T=95 ÞF (35 ÞC) X=0.10 to 0.90
		110,000 lbm/ft^2-hr (150 kg/m^2-sec)	T=95 ÞF (35 ÞC) X=0.10 to 0.90
		220,000 lbm/ft^2-hr (300 kg/m^2-sec)	T=95 ÞF (35 ÞC) X=0.10 to 0.90
		364,000 lbm/ft^2-hr (500 kg/m^2-sec)	T=95 ÞF (35 ÞC) X=0.10 to 0.90
R-32/125 with Ester Oil	1%	55,000 lbm/ft^2-hr (75 kg/m^2-sec)	T=95 ÞF (35 ÞC) X=0.10 to 0.90
		110,000 lbm/ft^2-hr (150 kg/m^2-sec)	T=95 ÞF (35 ÞC) X=0.10 to 0.90
		220,000 lbm/ft^2-hr (300 kg/m^2-sec)	T=95 ÞF (35 ÞC) X=0.10 to 0.90
		364,000 lbm/ft^2-hr (500 kg/m^2-sec)	T=95 ÞF (35 ÞC) X=0.10 to 0.90
	3%	55,000 lbm/ft^2-hr (75 kg/m^2-sec)	T=95 ÞF (35 ÞC) X=0.10 to 0.90
		110,000 lbm/ft^2-hr (150 kg/m^2-sec)	T=95 ÞF (35 ÞC) X=0.10 to 0.90
		220,000 lbm/ft^2-hr (300 kg/m^2-sec)	T=95 ÞF (35 ÞC) X=0.10 to 0.90
		364,000 lbm/ft^2-hr (500 kg/m^2-sec)	T=95 ÞF (35 ÞC) X=0.10 to 0.90
	5%	55,000 lbm/ft^2-hr (75 kg/m^2-sec)	T=95 ÞF (35 ÞC) X=0.10 to 0.90
		110,000 lbm/ft^2-hr (150 kg/m^2-sec)	T=95 ÞF (35 ÞC) X=0.10 to 0.90
		220,000 lbm/ft^2-hr (300 kg/m^2-sec)	T=95 ÞF (35 ÞC) X=0.10 to 0.90
		364,000 lbm/ft^2-hr (500 kg/m^2-sec)	T=95 ÞF (35 ÞC) X=0.10 to 0.90

Figure 4.1 Test Matrix

4.3.1 Start-up and Running Procedures

After performing numerous tests to find and stop any leaks within the test apparatus, a vacuum pump was attached to a charging valve and it evacuated the apparatus to as close to a total vacuum as can be managed. All valves were closed and opened again to loosen any trapped refrigerant or air, and the vacuum pump was left on overnight. When the system was ready to be charged with refrigerant, the receiver was valved off to isolate it from the rest of the apparatus. Then the apparatus, with the exception of the receiver, was fully charged with refrigerant until the system was filled with subcooled liquid. The receiver was then filled with refrigerant such that it was filled mostly with vapor, but also with a small amount of liquid. The reason that such care was taken with the receiver was that the receiver required enough refrigerant to perform subcooled liquid tests as well as enough volume to perform superheated vapor tests.

The water bath surrounding the receiver was then set with a temperature controlled heater to provide the desired saturation pressure in the system. Once the water bath reached the desired temperature, the valves to the various water circuits for the heat exchanger, after-condenser, and test section were opened. Then the refrigerant pump was turned on and set to the desired mass flux, after which the heaters for both the refrigerant and the water going to the diabatic test section were set to the desired levels. After a half hour or so the system stabilized, and it was ascertained that enough charge was in the system by confirming that the refrigerant flowing into the heater was subcooled.

As the refrigerant flowed from the test section to the receiver, there were two paths that it was able to flow through: The refrigerant could flow directly into the receiver, or it could flow through the aftercondenser and then into the receiver as shown in Figure 4.2. The flow was controlled using a valve on each path into the receiver, though generally the valve controlling the flow from the after-condenser was always left open. The heat to the refrigerant was gradually increased for each successively higher vapor quality test. This tended to increase the pressure, and thus the saturation temperature of the system. To bring the saturation temperature back down to the desired temperature, the receiver input control valve was tightened slightly, which caused more refrigerant to go through the after-condenser and thus would lower the saturation temperature to the desired level.

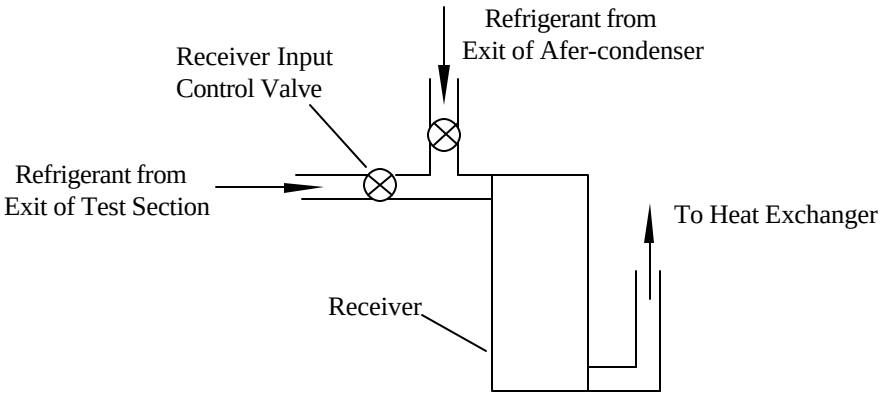

Figure 4.2--Refrigerant Flow Through the Receiver

Figure 4.2 Refrigerant Flow Through the Receiver

For each test, once the desired vapor quality, saturation temperature, and wall temperature difference was achieved, the data acquisition system was activated to save all pressure and temperature readings while the operator manually measured the rate of water flow through the test section and recorded the flow patterns of the refrigerant flowing through the sight glasses. After the tests were run, the data were reduced with a macro for the computer program, Excel 4.0, using the data reduction techniques described in Chapter 5.

4.3.2 Oil Injection and Concentration Measurement Procedures

The oil was injected into the apparatus using a special displacement pump, and then the oil-refrigerant mixture was pumped through the system at a high mass flux to uniformly mix the oil with the refrigerant. In order to calculate an estimate of how much oil was to be injected, the mass of the refrigerant entering the system during charging periods was measured, and then the mass of oil to be injected was calculated from Equation 4.1:

$$m_{oil} = \frac{\omega_{desired} \cdot m_{ref}}{1 - \omega_{desired}} \tag{4.1}$$

where $\omega_{desired}$ represents the desired mass fraction of the system. To determine the amount of oil that was actually being injected into the system, the mass of oil injected with each stroke of the pump was measured, and the number of strokes used to inject the oil was carefully monitored.

The method used to measure the apparatus' operating oil concentration was very different from the ASHRAE Standard 41.4 (ASHRAE, 1984). Since the refrigerant used in this study was in such short supply and not commercially available, special care had to be taken to assure that enough refrigerant would be available for the duration of the experiments. The ASHRAE Standard 41.4 mandates that a 1 lb. (455 g) sample be taken for each concentration measurement, which would limit the number of measurements that could be taken with the supply of refrigerant at hand. However, an alternative method was found in which a gas chromatograph analyzer was used to accurately measure very small amounts of oil from samples as small as 0.0066 lbs. (3 g). Thanks to this alternative method, this study includes an analysis of how the oil concentrations at fixed points in a closed loop can vary for different flow rates and qualities.

Before running the oil-refrigerant mixture tests, calibration of the oil used in this study was performed for the gas chromatograph analyzer. From the curve fit of the calibration data, the mass of oil in the sample can be found. The sample was taken by trapping the mixture while in liquid phase and weighing the sample device. Then the sample was flashed through a special set of filters that collect the oil, and the sampling device is weighed again in order to find the total mass of the sampled mixture. Any oil residue left on the container of the filters was wiped clean with the filter paper to make certain that all of the oil in the sample was collected. The filters were then placed in the gas chromatograph analyzer, which vaporizes the oil on the filters and determines the total mass of oil that was contained in the sample mixture. It should be noted that this method has been compared with the ASHRAE Standard 41.4, and has been found to be accurate to within 10% of the concentration found through the ASHRAE Standard. The oil concentration was calculated from the following equation:

$$\omega_o = \frac{m_{oil}}{m_{sample}} \tag{4.2}$$

Chapter 5: Data Reduction Techniques

This chapter discusses the methods used to reduce and evaluate the experimental data received from the condensation tests. The first part of this chapter discusses how the experimental values for the local convective heat transfer coefficients of the tube surface are found. Next, a discussion of the energy balance calculations for this study is provided. The last section of this chapter discusses the necessary changes in the data reduction techniques to account for the mixing of oil into the refrigerant.

5.1 Calculation of the Convective Heat Transfer Coefficients

In order to calculate the refrigerant-side convective heat transfer coefficient, h, Newton's law of cooling is used for all of the experiments in this study and is represented by the following equation:

$$h = \frac{q''}{\left(T_{\infty} - T_s\right)} \tag{5.1}$$

The convective heat flux from the surface of the tube is q", and the temperatures of the tube surface and fluid are T_s and T_{∞}, respectively. For the purposes of this study, the equation for the heat transfer coefficient becomes

$$h = \frac{q}{A_i\left(\overline{T}_{sat} - \overline{T}_{wall}\right)} \tag{5.2}$$

This equation assumes that the inside diameter, A_i, remains constant along the entire length of the condenser tube. q represents the total heat transfer out from the condenser, $\overline{T}_{sat}$ represents the average saturation temperature of the refrigerant in the test section, and $\overline{T}_{wall}$ represents the average wall temperature of the test section. $\overline{T}_{sat}$ and $\overline{T}_{wall}$ are found from the following equations:

$$\overline{T}_{sat} = \frac{T_{sat,in} + T_{sat,out}}{2}$$
$$T_{sat,in} = T_{sat}\left(P_{inlet}\right)$$
$$T_{sat,out} = T_{sat}\left(P_{inlet} + \Delta P_{TS}\right)$$

(5.3)

$$\overline{T}_{wall} = \frac{9*\left(T_{z=6} + T_{z=30}\right) + 6*\left(T_{z=12} + T_{z=18} + T_{z=24}\right)}{36}$$

The subscripts on the temperatures in the equation for the average wall temperature correspond to the average thermocouple reading at the position indicated by the subscript (i.e. "z=6" indicates the position 6 inches downstream from the inlet of the test section).

5.2 Energy Balance Calculations

The refrigerant flowing through the apparatus goes through the following thermodynamic cycle: Heat is input into the refrigerant as it passes through the heater, heat is removed from the refrigerant as it passes through the

condenser test section, and heat is removed again from the refrigerant in the after-condenser and in the heat exchanger in order to subcool the fluid before it is pumped through the cycle again. During these processes, there is heat loss to the environment, which must be known in order to quantify the exact inlet and outlet conditions of the refrigerant in the test section. These heat losses can be calculated from an energy balance of the system.

After the refrigerant passes through the pump, it is heated by external strip heaters to bring the refrigerant to the desired temperature and quality at the inlet to the test section. The enthalpy at the heater inlet is found by measuring the temperature and pressure at the heater inlet location and using the following equation:

$$h_{htr,in} = h_f + v_f\left[P_{htr,in} - P_{sat,htr,in}\right] \tag{5.4}$$

where h_f, v_f, and $P_{sat,htr,in}$ are the saturation values associated with the measured temperature at the heater inlet (Hinde, et al. 1993). The enthalpy at the inlet to the test section is then calculated from the following equation:

$$h_{TS,in} = h_{htr,in} + \frac{\dot{Q}_{htr} - \dot{Q}_{loss}}{\dot{m}_{ref}} \tag{5.5}$$

which uses the net heat input into the system per unit mass of refrigerant. The heat input by the heater is measured using a power transducer and the heat loss to the environment is calculated by the following equation:

$$\dot{Q}_{loss} = \frac{UA_{TS}\cdot\left(T_{wat,in} + T_{wat,out} - 2*T_{air}\right)}{2} \tag{5.6}$$

where UA_{TS} is measured from single-phase liquid tests as performed by Dobson et al. (1994).

The heat balance for the test condenser is calculated from the following equation:

$$\dot{Q}_{TS} = \left(\dot{m}_{wat}\, c_p \Delta T_{wat}\right) \tag{5.7}$$

where c_p is the specific heat of water at the average temperature of the water inlet and outlet. The enthalpy of the refrigerant is calculated from the following equation using the calculated heat removed from the test section in Equation 5.7.:

$$h_{TS,out} = h_{TS,in} - \frac{\dot{Q}_{TS}}{\dot{m}_{ref}} \tag{5.8}$$

The vapor qualities at the inlet and outlet of the test condenser are calculated using enthalpies in the following equations:

$$x_{in} = \frac{h_{TS,in} - h_f\left(T_{sat,in}\right)}{h_{fg}\left(T_{sat,in}\right)} \tag{5.9a}$$

$$x_{out} = \frac{h_{TS,out} - h_f\left(T_{sat,out}\right)}{h_{fg}\left(T_{sat,out}\right)} \tag{5.9b}$$

where h_f is the saturated liquid enthalpy and h_{fg} is the difference between the saturated vapor enthalpy and the saturated liquid enthalpy. The vapor quality is assumed to change linearly along the length of the test section in this

study since only small quality changes are experienced between the inlet and outlet of the test section. Therefore, the average vapor quality of the test section is calculated from the following equation:

$$\bar{x} = \frac{x_{in} + x_{out}}{2} \tag{5.10}$$

5.3 Adjustments for Oil Effects

One of the major effects of mixing oil with refrigerant is that the oil causes the effective saturation temperature to change by a quantity called "apparent superheat". This phenomenon causes the measured experimental saturation temperature to deviate higher than the saturation temperature calculated from the saturation pressure curve, which in the case of this study deviated as high as 7 °R (3.9 K) for inlet qualities of 95%, and thus required measurements to be based on an adjusted saturation temperature. Besides the apparent superheat adjustment, the properties of the liquid component of the two-phase mixture must be adjusted using the mixing laws mentioned in Chapter 2.

The apparent superheat is measured experimentally for this study instead of using Raoult's law since the inlet and outlet temperature measurements are fairly accurate. Also, in a past study performed by Eckles, Zoz, and Pate (1991), it was found that Raoult's law tended to overestimate the changing saturation temperature by 100%, which leaves some skepticism about its accuracy. Curve fits of the apparent superheat values with respect to quality, $\Delta T_{AS}(x)$, were used to help solve for the average saturation Temperature, $\bar{T}_{sat}$, as shown by the following equations:

$$\Delta T_{AS}(x) = T_{in} - T_{sat,in}(P_{in})$$

$$T_{sat,out} = T_{sat,in}(P_{in}) - \frac{dT}{dP}\Delta P_{TS} + \Delta T_{AS,out}(x_{out})$$

$$\bar{T}_{sat} = \frac{T_{inlet} + T_{sat,out}}{2} \tag{5.11}$$

In the data reduction, the properties of the liquid portion of the two-phase mixture were adjusted since the oil is assumed to remain entirely in the liquid phase of the mixture due to its very low vapor pressure. This method requires the calculation of the mass fraction of oil in the liquid phase of the refrigerant and is calculated using the known oil concentration and quality of the two-phase mixture. The equation used to calculate the oil concentration in the liquid phase of the refrigerant, $\omega_{o,l}$, is the following:

$$\omega_{o,l} = \frac{m_{oil}}{m_l} = \frac{\omega_o}{1 - x} \tag{5.12}$$

The above equation is used with the equations presented in Chapter 2 that account for mixture effects upon the refrigerant thermodynamic properties.

Chapter 6: Experimental Results

This chapter presents the experimental results of the tests performed using R-32/125, both pure and mixed with an oil at various concentrations as specified in Chapter 4. The experimental results are then compared with a number of previously developed correlations for both the heat transfer coefficient and the pressure drop per unit length during condensation. The data for all of the tests run is organized in tabular form in Appendix B.

6.1 Results for Pure R-32/125

The experimental values for the heat transfer coefficient are plotted versus vapor quality in Figure 6.1. This graph shows the typical monotonically increasing trend of the heat transfer coefficient with quality. The slope is fairly flat at the lower mass fluxes since the stratified and wavy flow regimes are encountered at the lower mass fluxes of 55 and 110 klb/ft^2-hr (75 and 150 kg/m^2-s). For the higher mass fluxes of 220 and 364 klb/ft^2-hr (300 and 500 kg/m^2-s), with the exception of low qualities (x<0.4), the refrigerant flows in the annular regime, which typically causes h to increase faster with increasing quality since the vapor shear thins the liquid annular film and thus helps facilitate heat transfer.

The predictions of a number of correlations are plotted as lines superimposed with the experimental data in Figures 6.2 through 6.5, each figure representing a different mass flux. Figures 6.2 and 6.3 show that the Dobson correlation predicts the data very well, and that the Chato correlation appears to predict the average value of h, though the Chato correlation is meant only for the stratified flow regime. The Traviss, Cavalini-Zecchin, Shah, and Chen correlations predict the heat transfer coefficient poorly since they make the assumption of annular flow, though for these two mass fluxes the stratified and wavy flow regimes are primarily encountered.

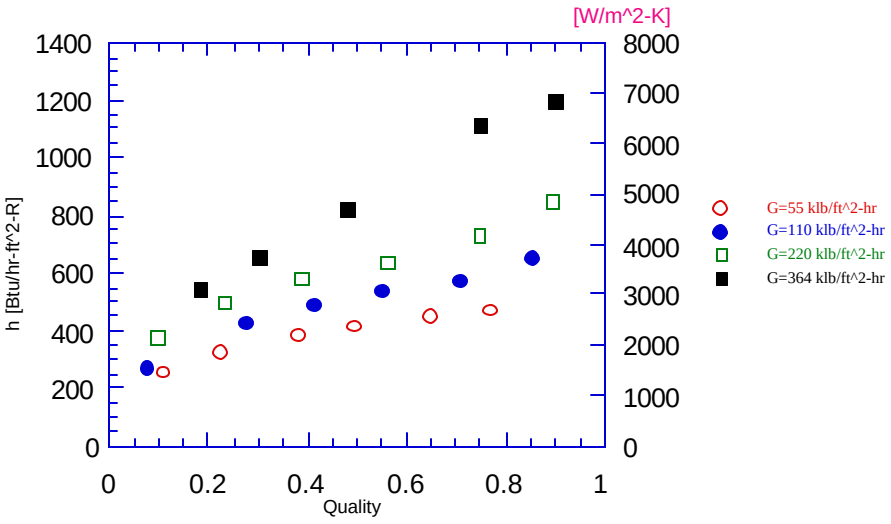

Figure 6.1 Experimental Values of the Heat Transfer Coefficient for Pure R-32/125

In Figures 6.4 and 6.5, however, the data shown is for the higher two mass fluxes and are mostly either in the annular or annular-wavy flow regime, so the annular flow-based correlations show a marked improvement in their predictions. The Dobson, Cavalini-Zecchin, and Traviss correlations seem to predict the experimental data very well,

though the Chen correlation consistently underpredicts the data. The predicted values of the correlations are then plotted versus the experimental values of h in Figures 6.6 through 6.9. These graphs show the predictions' performances in a more quantifiable manner. As can be seen in Figure 6.6, the Dobson correlation fits the data almost perfectly. The data for the mass flux of 110 klb/ft^2-hr (150 kg/m^2-s) is shown in Figure 6.7, and the annular flow correlations can be seen to start to approach the experimental values, which can be explained by the fact that at this mass flux, the annular-wavy flow pattern is encountered. Just as in Figures 6.4 and 6.5, Figures 6.8 and 6.9 show how the Traviss, Cavalini-Zecchin, Shah, and Dobson correlations do a fairly good job of predicting the heat transfer coefficient, with the Dobson and Cavalini-Zecchin correlations performing the best of the correlations presented here. The Chen correlation, on the other hand, underpredicts the experimental data by over 20%. In Figures 6.4 and 6.5 the Chato correlation is shown only for reference purposes because it should not be used with high mass fluxes.

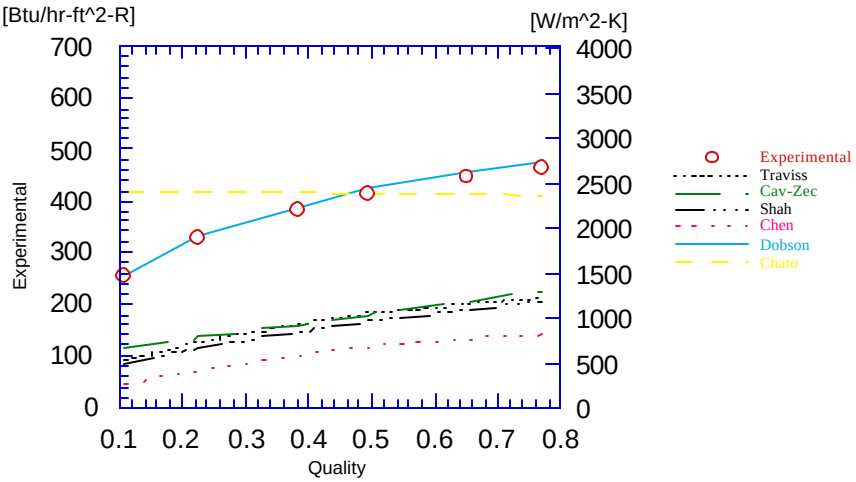

Figure 6.2 Comparison of Heat Transfer Coefficient Correlations with Respect to Quality for R-32/125 at a Mass Flux of 55 klb/ft^2-hr (75 kg/m^2-s)

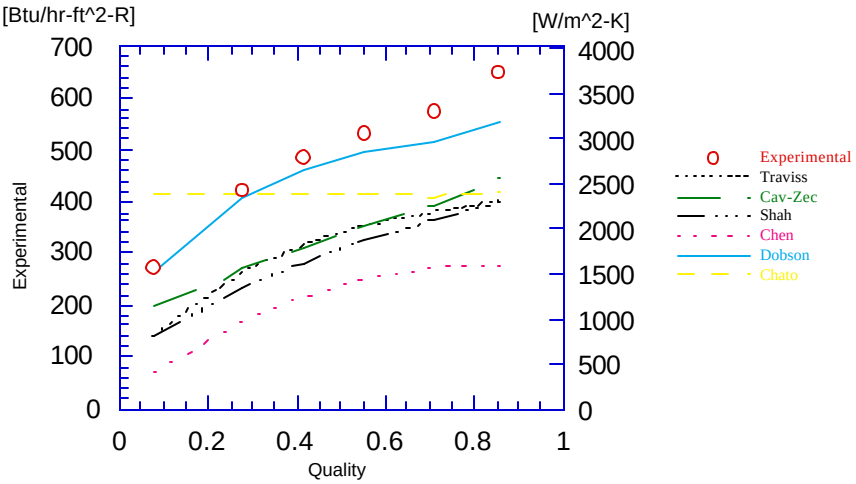

Figure 6.3 Comparison of Heat Transfer Coefficient Correlations with Respect to Quality for R-32/125 at a Mass Flux of 110 klb/ft^2-hr (150 kg/m^2-s)

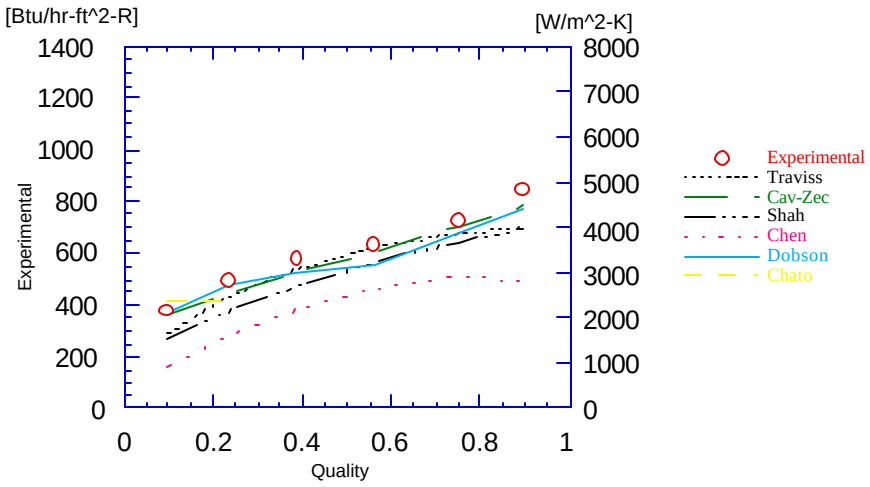

Figure 6.4 Comparison of heat Transfer Coefficient Correlations with Respect to Quality for R-32/125 at a Mass Flux of 220 klb/ft^2-hr (300 kg/m^2-s)

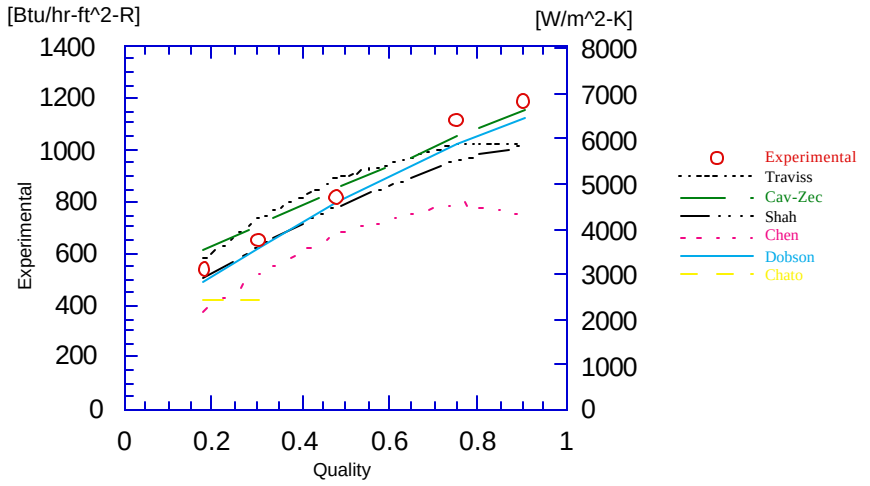

Figure 6.5 Comparison of Heat Transfer Coefficient Correlations with Respect to Quality for R-32/125 at a Mass Flux of 364 klb/ft^2-hr (500 kg/m^2-s)

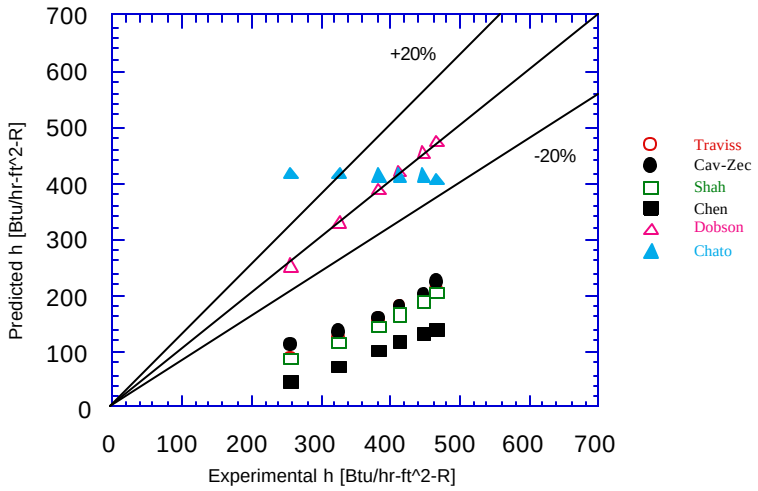

Figure 6.6 Predicted vs. Experimental Values of the Heat Transfer Coefficient for R-32/125 at a Mass Flux of 55 klb/ft^2-hr (75 kg/m^2-s)

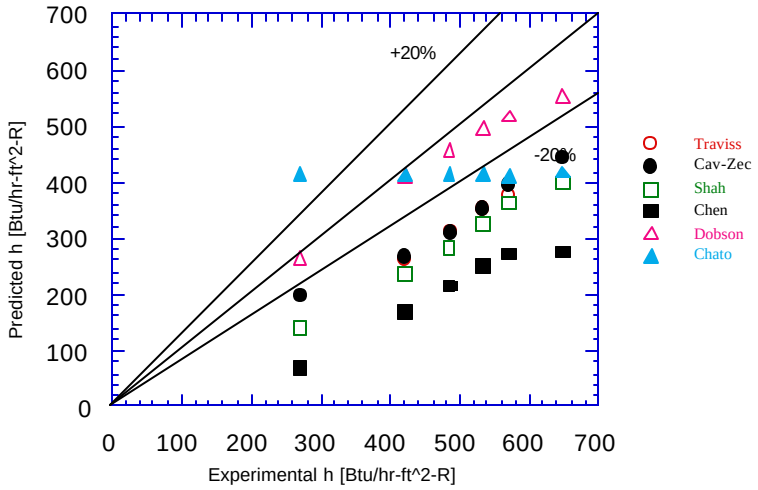

Figure 6.7 Predicted vs. Experimental Values of the Heat Transfer Coefficient for R-32/125 at a Mass Flux of 110 klb/ft^2-hr (150 kg/m^2-s)

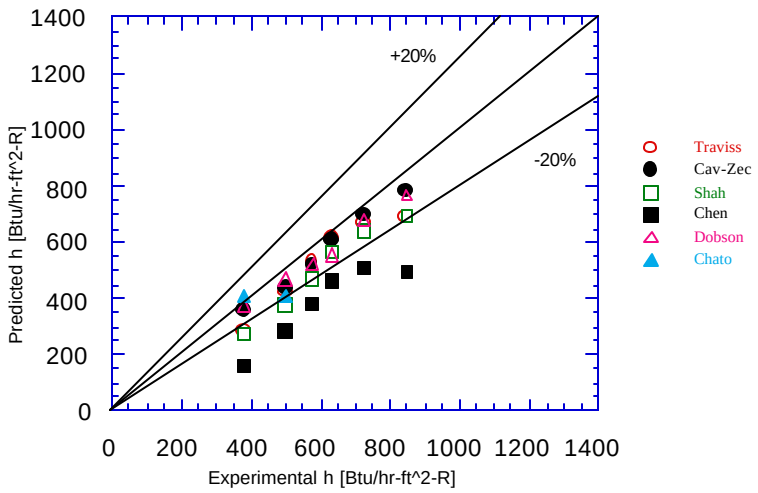

Figure 6.8 Predicted vs. Experimental Values of the Heat Transfer Coefficient for R-32/125 at a Mass Flux of 220 klb/ft^2-hr (300 kg/m^2-s)

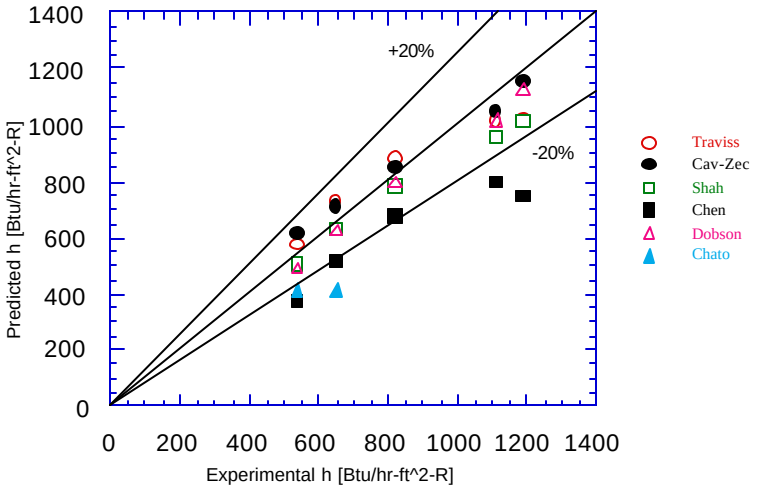

Figure 6.9 Predicted vs. Experimental Values of the Heat Transfer Coefficient for R-32/125 at a Mass Flux of 364 klb/ft^2-hr (500 kg/m^2-s)

The experimental pressure drop per unit length of the test section can be seen in Figure 6.10, which shows data for the higher mass fluxes of 220 and 364 klb/ft^2-hr (300 and 500 kg/m^2-s). For the lower mass fluxes, the magnitude of the pressure drop approaches the uncertainty of the pressure transducers, and therefore are not presented here. The pressure drop can be seen to increase smoothly with increasing quality, and that the pressure drop is greater for the mass flux of 364 klb/ft^2-hr (500 kg/m^2-s) than for 220 klb/ft^2-hr (300 kg/m^2-s).

To compare the experimental pressure drop with a previously developed correlation, the Souza correlation is plotted with the experimental data in Figure 6.11. The Souza correlation shows that the pressure drop should decrease once high vapor qualities (x>0.70) are experienced, though the experimental data does not show this phenomenon.

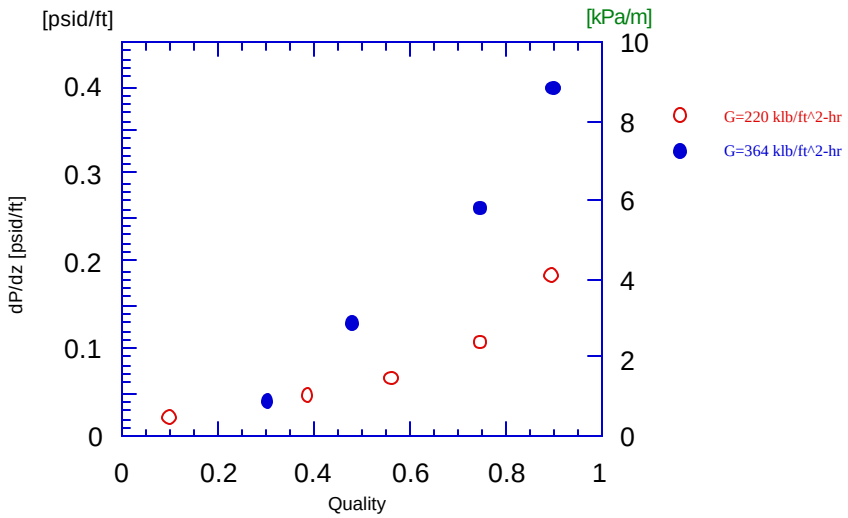

Figure 6.10 Experimental Pressure Drop of Pure R-32/125 vs. Quality

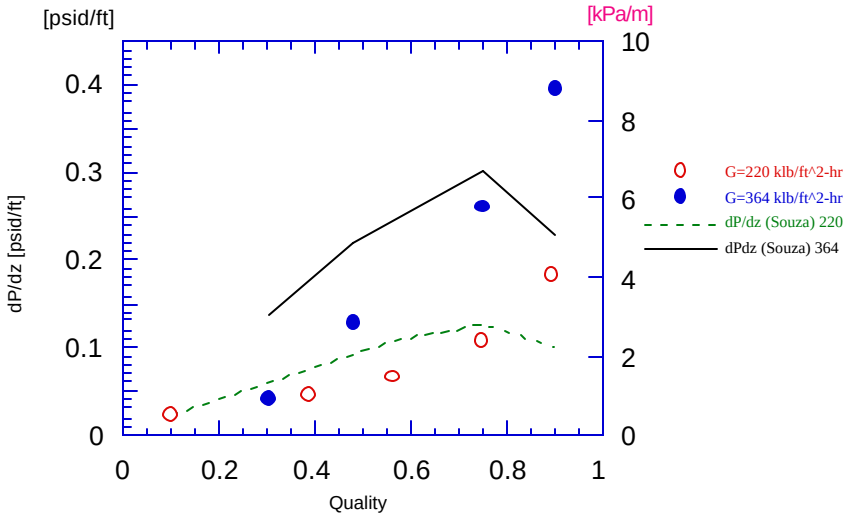

Figure 6.11 Comparison of Experimental Pressure Drop with the Souza Correlation for Pure R-32/125

6.2 Results for Oil Mixtures

The tests run for the oil-refrigerant mixtures were performed for average concentrations of 0.92%, 2.81%, and 5.50%, which are referred to, respectively, as 1%, 3%, and 5% in the graph legends for simplicity's sake. The average concentrations are calculated averages of the oil-refrigerant samples taken using the gas chromatography analyzer as discussed later. The addition of oil to pure refrigerant causes a phenomenon called apparent superheat, which is the increase in the saturation temperature of the oil-refrigerant mixture. This increase in the saturation temperature is plotted for each oil concentration in Figures 6.12 through 6.14, and was obtained experimentally. It can be seen that in each of the graphs, the apparent superheat increases approximately linearly with vapor quality. Another interesting trend to note is that for each of the graphs the apparent superheat is higher for increased mass flux. This trend suggests that either the apparent superheat is dependent on mass flux or that the higher mass fluxes tend to

circulate the oil in the system more uniformly, increasing the effective oil concentration and preventing the oil from collecting in stagnant areas. This trend is a very consistent trend with the exception of the 3% oil data in Figure 6.13, though the only deviation in this case is that the 220 klb/ft^2-hr (300 kg/m^2-s) data shows a higher superheat than the 364 klb/ft^2-s (500 kg/m^2-s) data. Though the data demonstrates linear relationships, it should be noted that the apparent superheat examined at vapor qualities greater than 95% for the 3% and 5% tests showed dramatic increases as high as 7 °R (3.9 °K). The reason for this increase is that there will always be a liquid phase of oil since the oil's boiling point is much higher than the refrigerant's saturation temperature, so the condition of single phase vapor can not be achieved until the boiling point of the oil is reached. In this study the saturation temperature was 90 °F (35 °C) while the boiling point of the oil used in this study is 480 °F (250 °C).

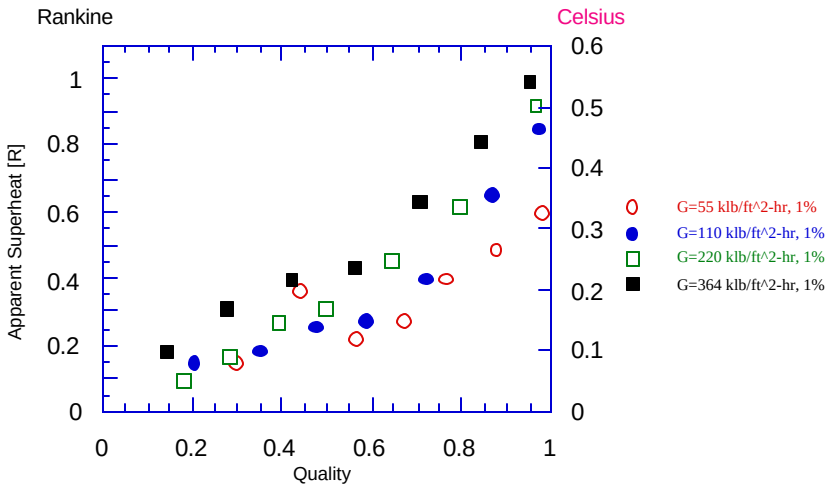

Figure 6.12 Graph of Apparent Superheat for R-32/125 Mixture with Approximately 1% Oil

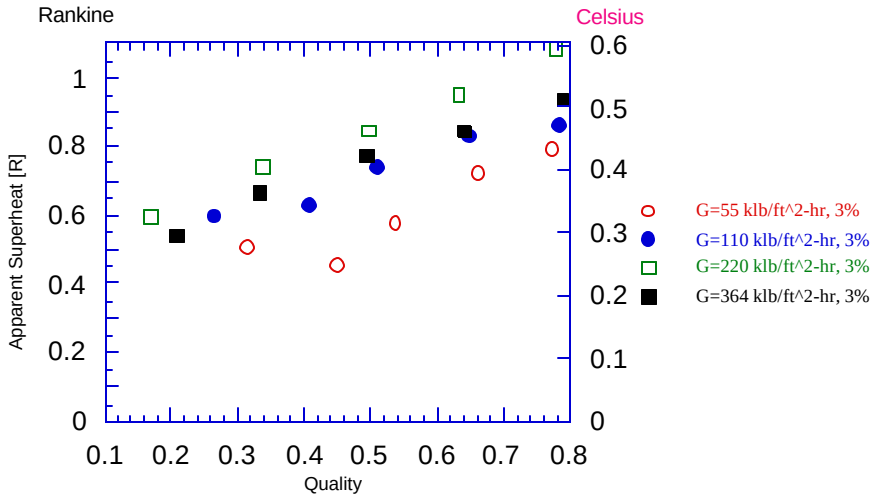

Figure 6.13 Graph of Apparent Superheat for R-32/125 Mixture with Approximately 3% Oil

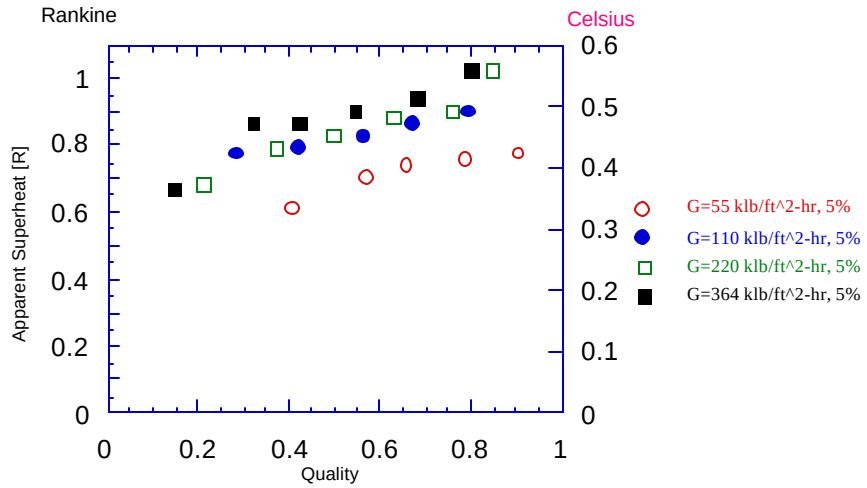

Figure 6.14 Graph of Apparent Superheat for R-32/125 Mixture with Approximately 5% Oil

The graph of the oil sample measurements taken during this study can be seen in Figure 6.15. Samples were taken for each of the four mass fluxes tested, and two samples were taken at each mass flux for the 1% and 3% oil concentrations, one sample at low vapor quality and one sample at high vapor quality. From this graph it can be seen that the oil concentration varies with different mass fluxes as well as different qualities. An explanation for this variation in concentration is that oil can collect in stagnant areas or wet the surfaces of any section of the apparatus that is in a vapor phase, particularly the receiver and heater sections. For the 3% data, the oil concentration measurements were consistently higher at the lower qualities, which could be explained by the fact that at lower qualities more liquid is flowing through the system and can carry more oil along with the liquid. At the 5% oil concentration, the method used for sampling shows a much larger variation in its results, which suggests that perhaps a larger sample or different sampling method should be used for this high oil concentration. An ASHRAE standard sample was also performed for the 5% oil concentration, and the result showed the concentration to be 5.5%, which was very close to the sampled average of 5.68%. Another observation that can be made from this data is that at the 1% oil concentration the lowest mass flux shows that very little of the oil in the system is flowing with the refrigerant, whereas at the higher mass fluxes the measured oil concentration is consistently around 1%.

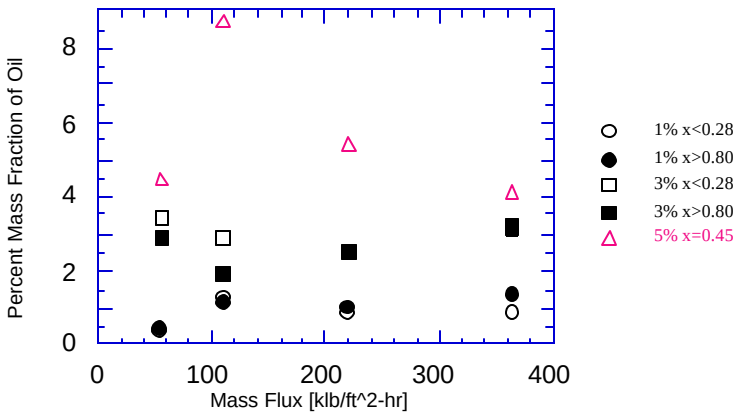

Figure 6.15 Oil Sample Measurements at Various Mass Fluxes and Qualities

The experimental results of the heat transfer coefficient, h, for all tests performed can be seen for each mass flux in Figures 6.16 through 6.19. All of the data points in these four graphs have been adjusted for apparent superheat and the effects of oil addition can clearly be seen. As can be seen in Figure 6.16, at the mass flux of 55 klb/ft^2-hr (75 kg/m^2-s) the oil addition causes no noticeable effect at the 1% oil concentration, though at 3% and 5% oil concentrations h shows some degradation. At the higher mass fluxes, it can be seen how h rises consistently with quality until the quality is approximately 40-50%. After reaching that quality range, the degradation in h due to oil begins to manifest itself. This decrease in h can be greater than 50% at qualities above 80%. It is interesting to note that at oil concentrations of 3% and 5% an enormous amount of foaming or frothing of bubbles was observed in the liquid portion of the two-phase mixture at qualities greater than 40%, which may have a connection to this large decrease in h.

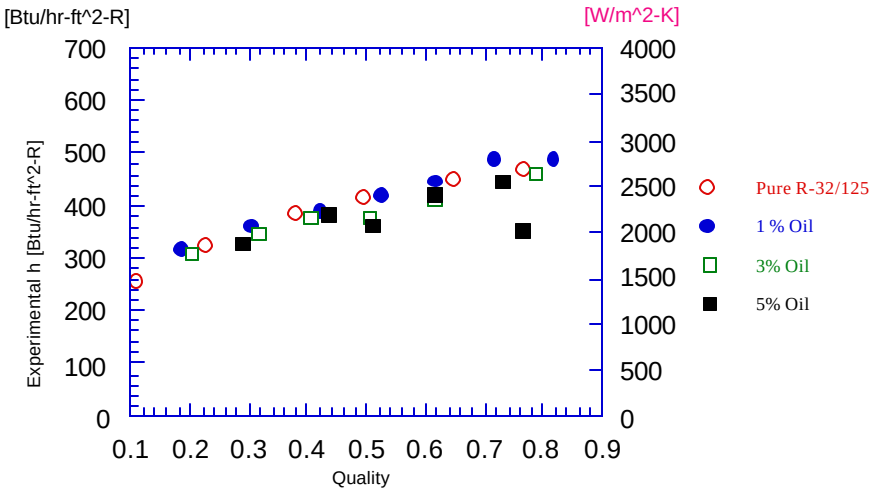

Figure 6.16--Experimental Values of the Heat Transfer Coefficient vs. Quality for R-32/125 at G=55 klb/ft^2-hr (75 kg/m^2-s)

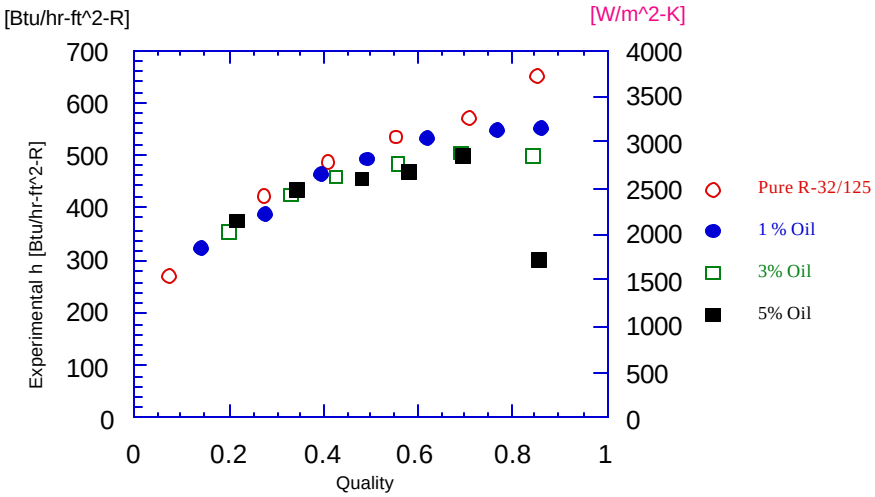

Figure 6.17 Experimental Values of the Heat Transfer Coefficient vs. Quality for R-32/125 at G=110 klb/ft^2-hr (150 kg/m^2-s)

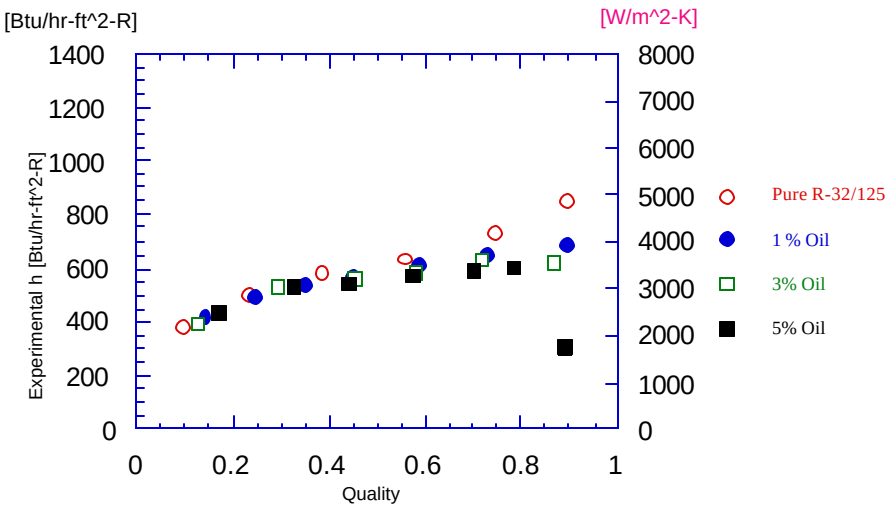

Figure 6.18 Experimental Values of the Heat Transfer Coefficient vs. Quality for R-32/125 at G=220 klb/ft^2-hr (300 kg/m^2-s)

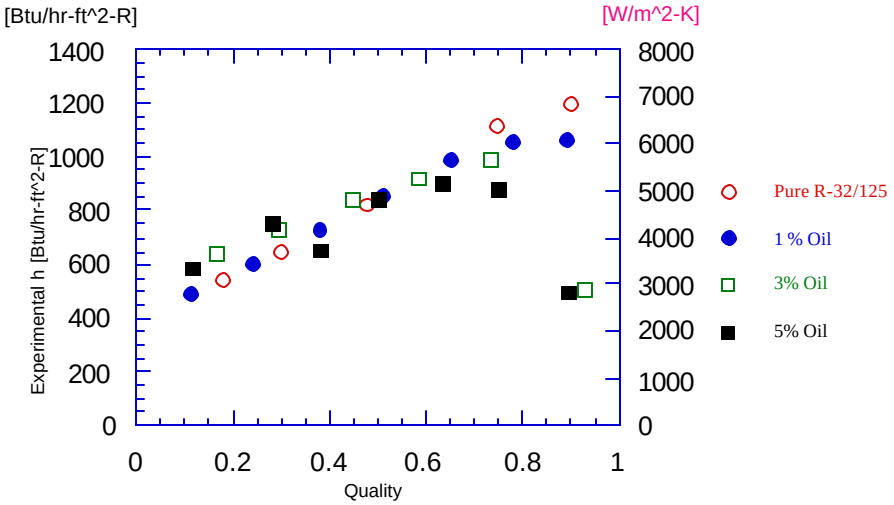

Figure 6.19 Experimental Values of the Heat Transfer Coefficient vs. Quality for R-32/125 at G=364 klb/ft^2-hr (500 kg/m^2-s)

The graphs in Figures 6.20 through 6.25 show the differences in the values of h when the apparent superheat is either neglected or taken into account. It seems that by neglecting the apparent superheat, the measured values of h may be as much as 10% higher than what they actually are. Also, if any of these curves are compared with the pure data shown in Figure 6.1, it can be seen that the slope of h vs. x decreases at qualities greater than 50%. It may be interesting to note that the 5% oil concentration data in Figures 6.24 and 6.25 have fairly flat profiles, even for the higher mass fluxes where annular flow would normally cause h to increase with x at a much greater rate. Even the highest mass flux shows results that would normally be experienced in the wavy flow regime. The foaming that occurs at the higher oil concentrations may be responsible for this behavior.

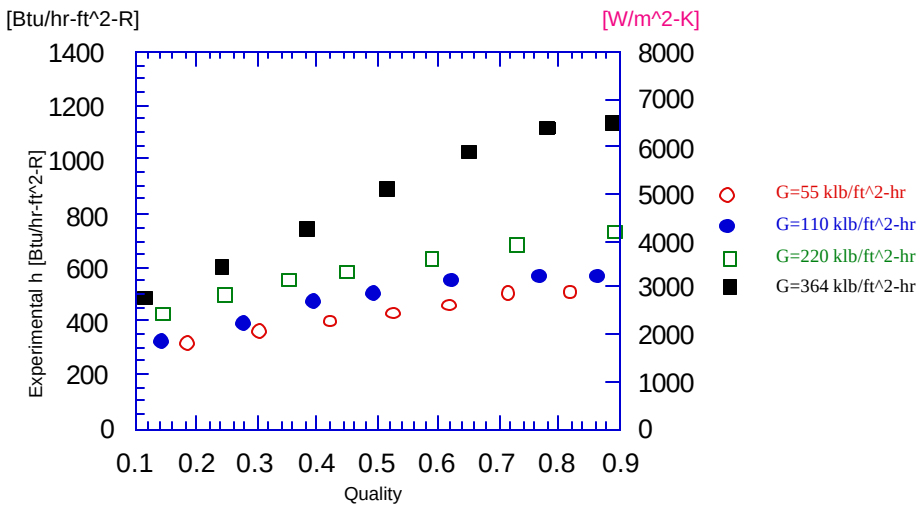

Figure 6.20 Experimental Values of the Heat Transfer Coefficient vs. Quality for R-32/125 Mixed with 1% Oil (Unadjusted for Oil Effects)

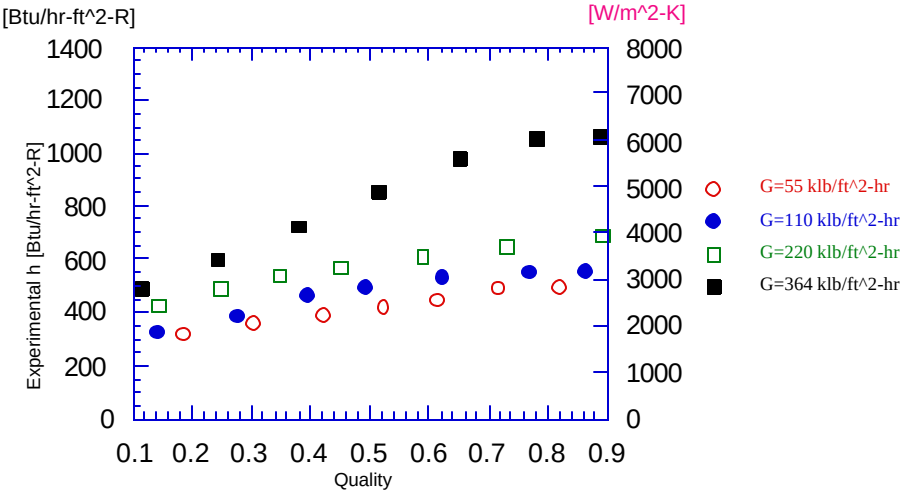

Figure 6.21 Experimental Values of the Heat Transfer Coefficient vs. Quality for R-32/125 Mixed with 1% Oil (Adjusted for Oil Effects)

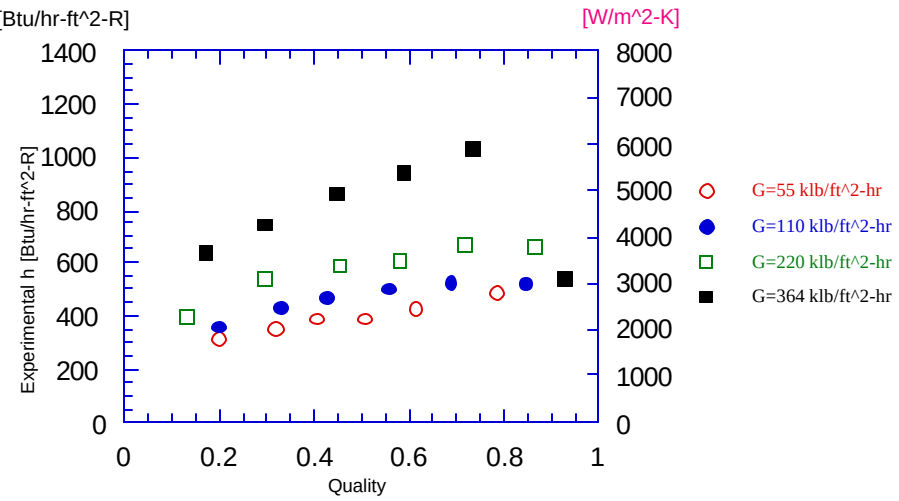

Figure 6.22 Experimental Values of the Heat Transfer Coefficient vs. Quality for R-32/125 Mixed with 3% Oil (Unadjusted for Oil Effects)

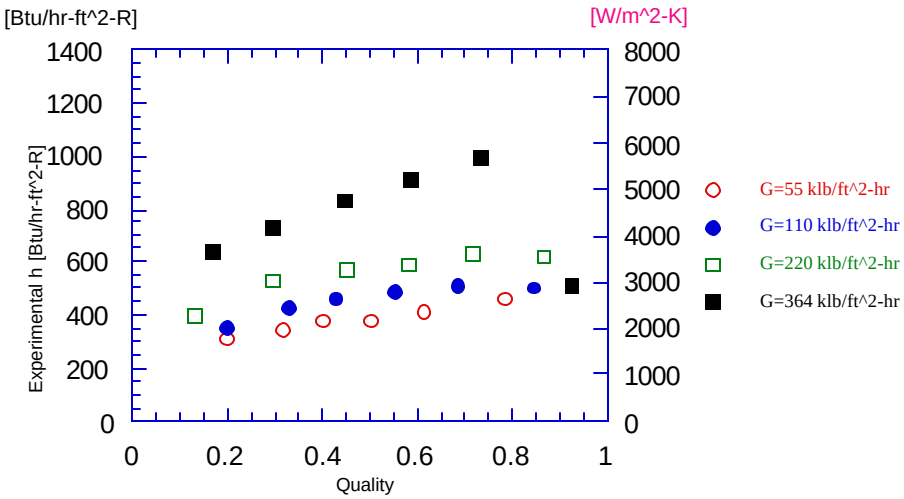

Figure 6.23 Experimental Values of the Heat Transfer Coefficient vs. Quality for R-32/125 Mixed with 3% Oil (Adjusted for Oil Effects)

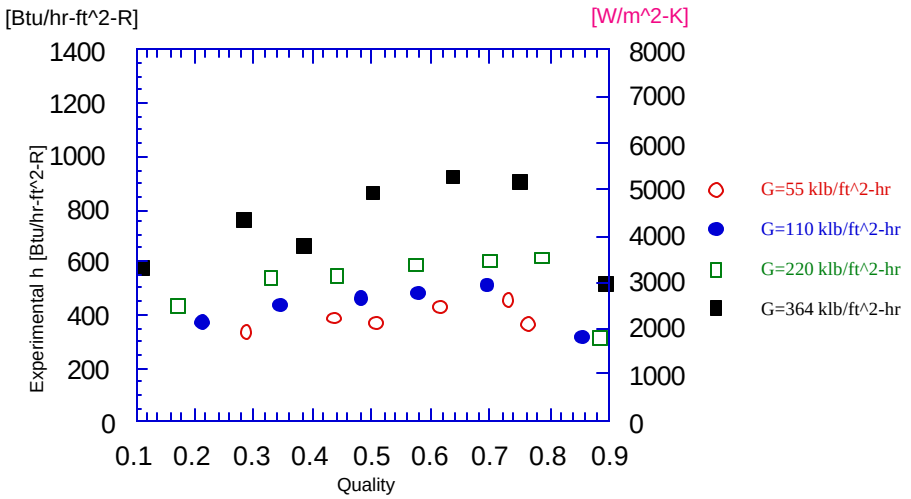

Figure 6.24 Experimental Values of the Heat Transfer Coefficient vs. Quality for R-32/125 Mixed with 5% Oil (Unadjusted for Oil Effects)

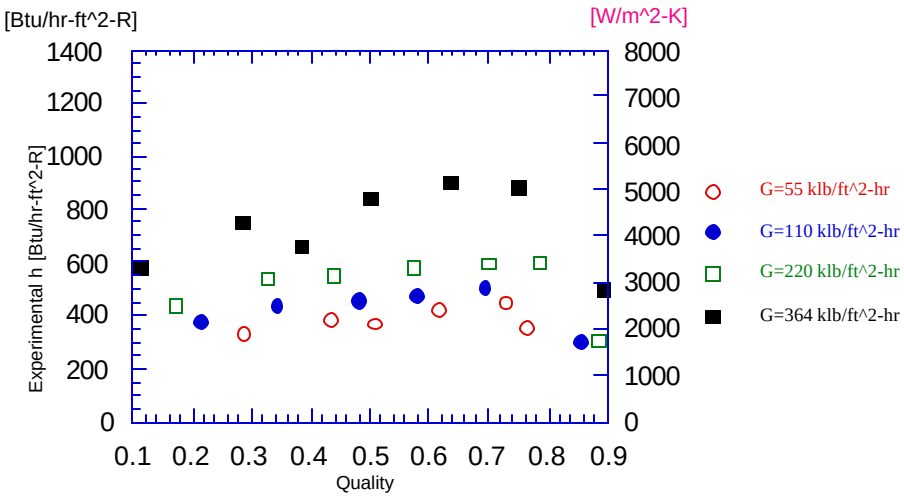

Figure 6.25 Experimental Values of the Heat Transfer Coefficient vs. Quality for R-32/125 Mixed with 5% Oil (Adjusted for Oil Effects)

If the heat transfer coefficient of oil-refrigerant mixtures could be predicted by the pure correlations, there would be little or no need for special enhancement factors to correct for the oil addition. Figures 6.26 through 6.31 show comparisons of the pure correlations with the experimental values of h, though for these graphs in particular the properties used in the correlations neglected the oil mixture effects. Figures 6.32 through 6.37 are the same as Figures 6.26 through 6.31 with the exception that oil mixing effects were included for the properties before using the correlation predictions.

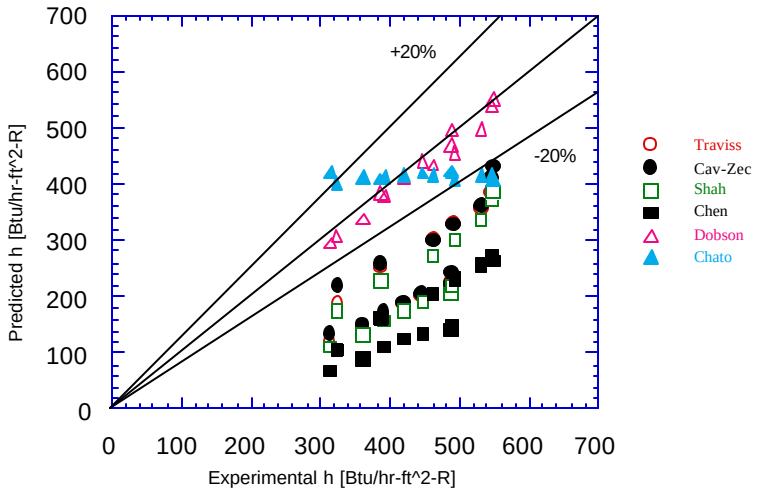

Figure 6.26 Predicted vs. Experimental Values of the Heat Transfer Coefficient for R-32/125 (1% Oil) at 55 and 110 klb/ft^2-hr (75 and 150 kg/m^2-s)

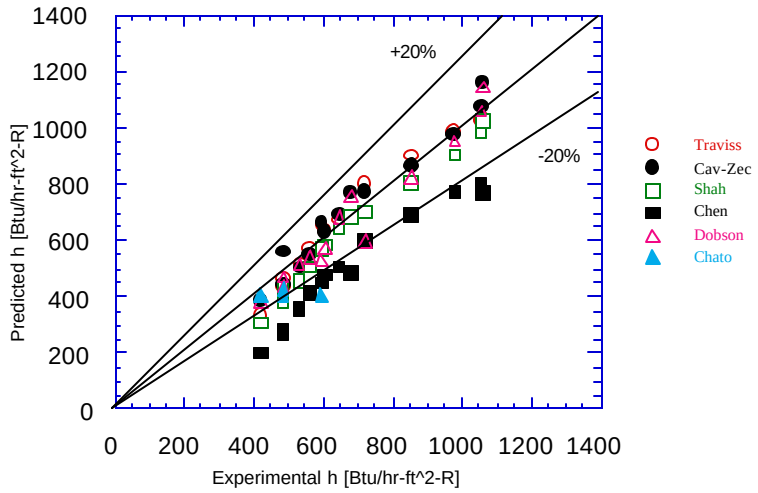

Figure 6.27 Predicted vs. Experimental Values of the Heat Transfer Coefficient for R-32/125 (1% Oil) at 220 and 364 klb/ft^2-hr (300 and 500 kg/m^2-s)

In Figures 6.26 and 6.27 the results look virtually the same as the results plotted in Figures 6.6 though 6.9, demonstrating that for oil concentrations of 1% or less the pure correlations can be used to obtain equally valid results. Again, the Dobson correlation shows excellent agreement with the experimental values for both low and high mass fluxes. The 3% oil concentration data are plotted in Figures 6.28 and 6.29, which show similar results as the 1% data. However, for the high mass fluxes it can be seen in Figures 6.29 and 6.31 that there are one or two points that are greatly overpredicted by almost all of the correlations, and these data points are where the quality had surpassed 90%, which can be deduced from looking once again at Figures 6.22 through 6.25. This occurrence can be seen to a greater degree for the 5% data in Figures 6.30 and 6.31, though the correlations still show similar agreement as before.

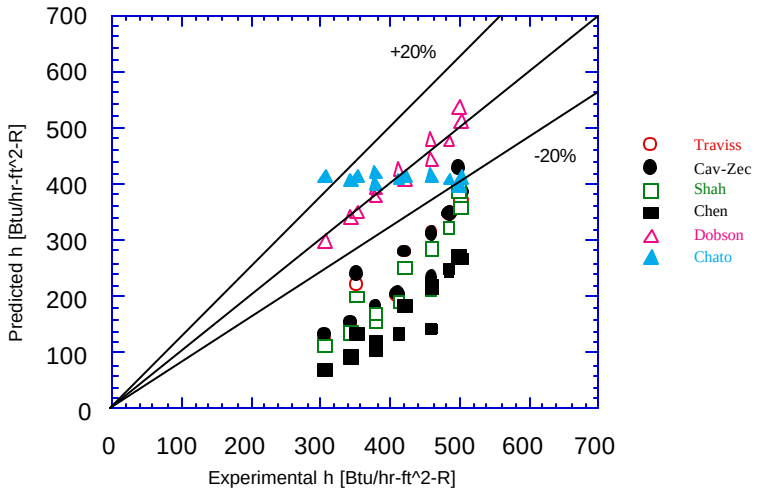

Figure 6.28 Predicted vs. Experimental Values of the Heat Transfer Coefficient for R-32/125 (3% Oil) at 55 and 110 klb/ft^2-hr (75 and 150 kg/m^2-s)

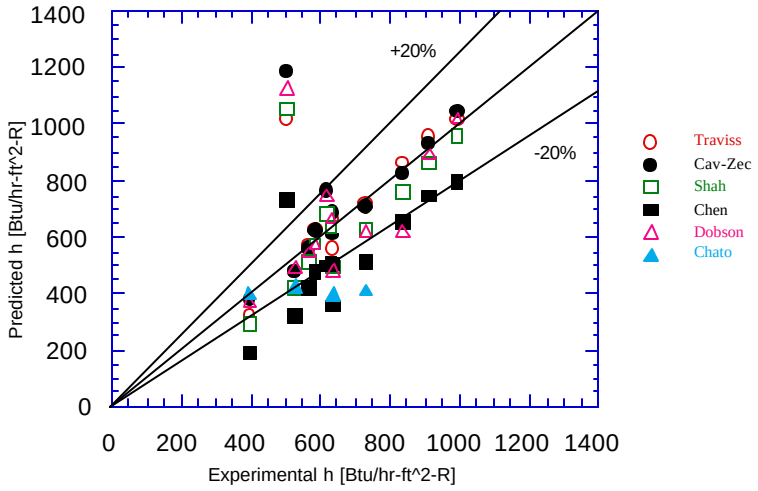

Figure 6.29 Predicted vs. Experimental Values of the Heat Transfer Coefficient for R-32/125 (3% Oil) at 220 and 364 klb/ft^2-hr (300 and 500 kg/m^2-s)

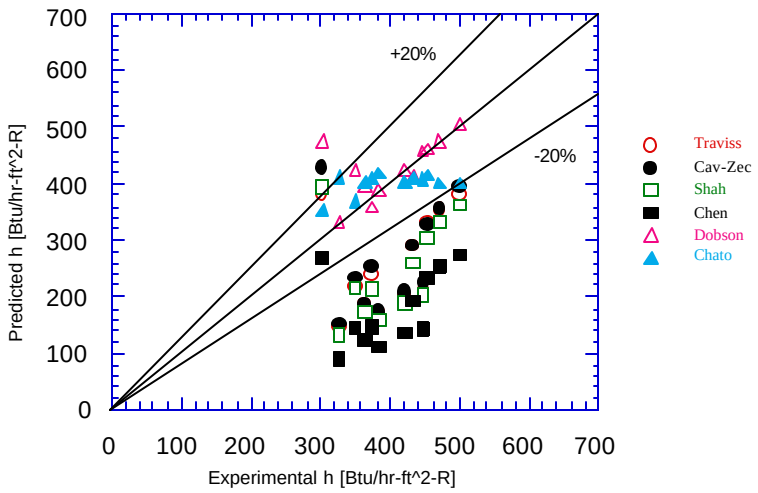

Figure 6.30 Predicted vs. Experimental Values of the Heat Transfer Coefficient for R-32/125 (5% Oil) at 55 and 110 klb/ft^2-hr (75 and 150 kg/m^2-s)

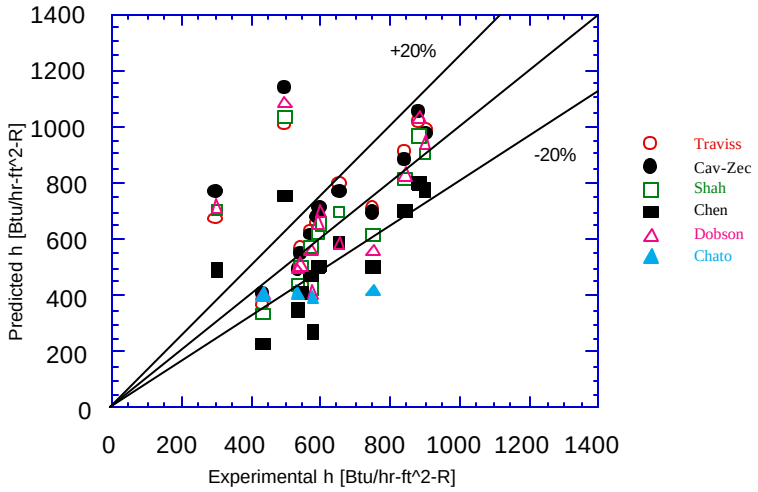

Figure 6.31 Predicted vs. Experimental Values of the Heat Transfer Coefficient for R-32/125 (5% Oil) at 220 and 364 klb/ft^2-hr (300 and 500 kg/m^2)

Figures 6.32 through 6.37 show the same correlation comparisons, except that the oil mixture effects were included in calculating the refrigerant properties before using the correlations. The equations used for calculating these properties can be found in Chapter 2. It can be seen that in all six of these graphs the inclusion of oil mixture effects upon the properties caused the correlations to perform much poorer than if the refrigerant was assumed to be pure. One of the possible causes for this poor performance is the tremendous change in the liquid viscosity due to oil addition. These graphs show that the correlations will underpredict the experimental values as more oil is added to the system. As can be seen in Figure 6.37, the oil concentration of 5% causes the correlations to underpredict h by at least 20%.

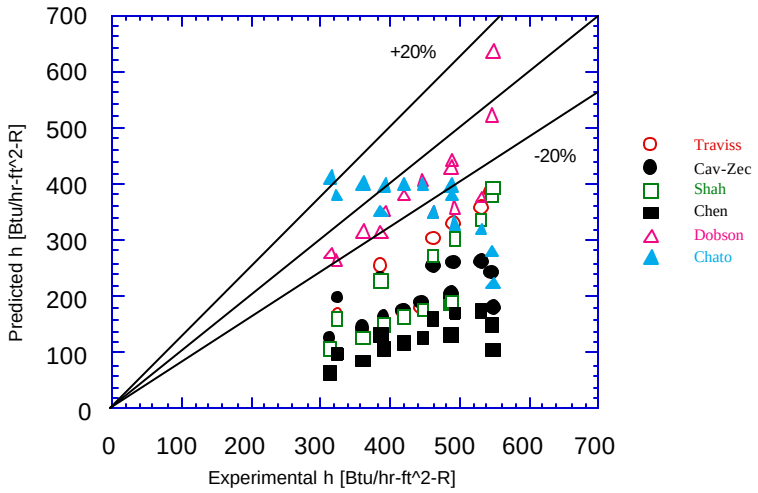

Figure 6.32 Predicted vs. Experimental Values of the Heat Transfer Coefficient for R-32/125 (1% Oil) at 55 and 110 klb/ft^2-hr (75 and 150 kg/m^2-s)--Properties Adjusted for Mixture Effects

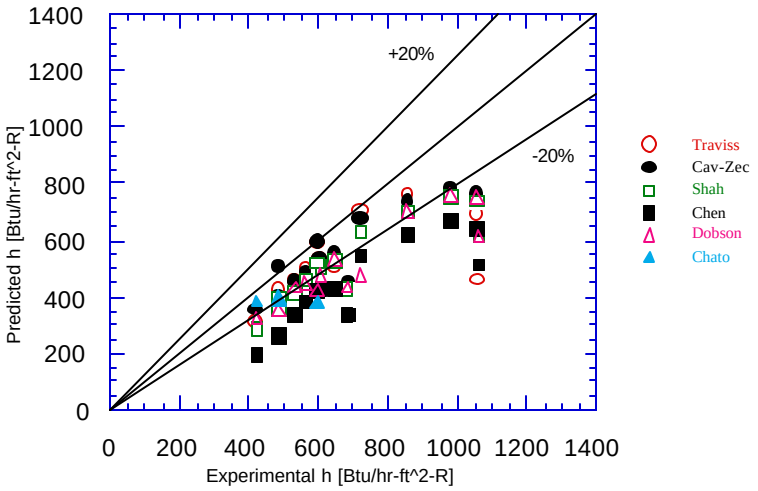

Figure 6.33 Predicted vs. Experimental Values of the Heat Transfer Coefficient for R-32/125 (1% Oil) at 220 and 364 klb/ft^2-hr (300 and 500 kg/m^2-s)--Properties Adjusted for Mixture Effects

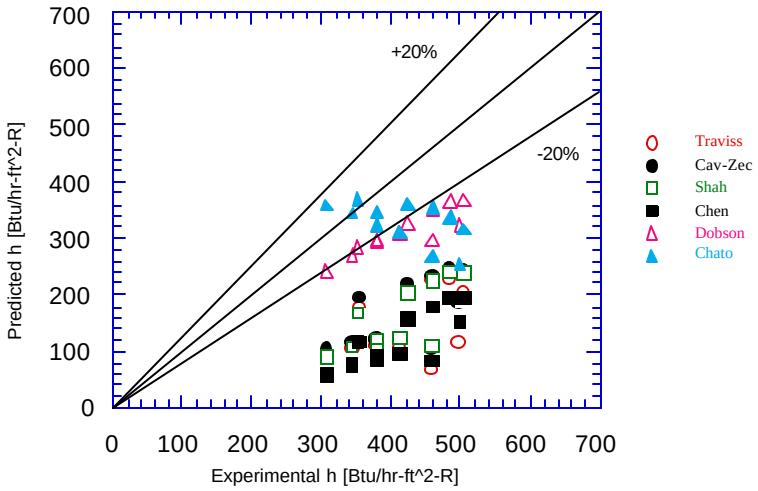

Figure 6.34 Predicted vs. Experimental Values of the Heat Transfer Coefficient for R-32/125 (3% Oil) at 55 and 110 klb/ft^2-hr (75 and 150 kg/m^2-s)--Properties Adjusted for Mixture Effects

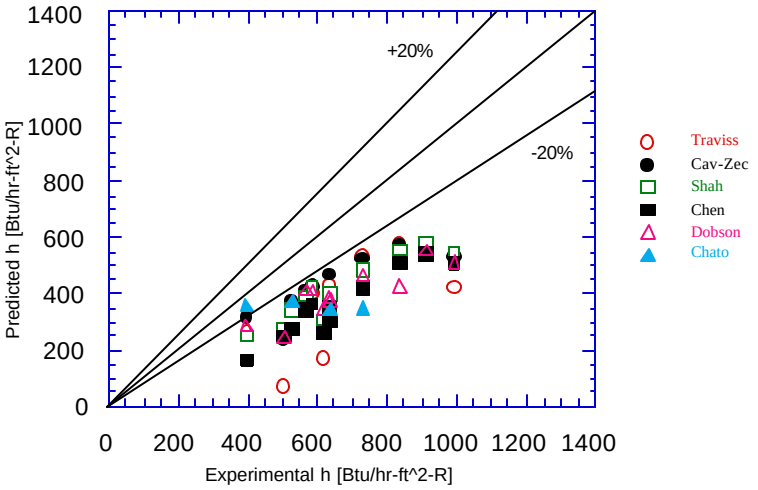

Figure 6.35 Predicted vs. Experimental Values of the Heat Transfer Coefficient for R-32/125 (3% Oil) at 220 and 364 klb/ft^2-hr (300 and 500 kg/m^2-s)--Properties Adjusted for Mixture Effects

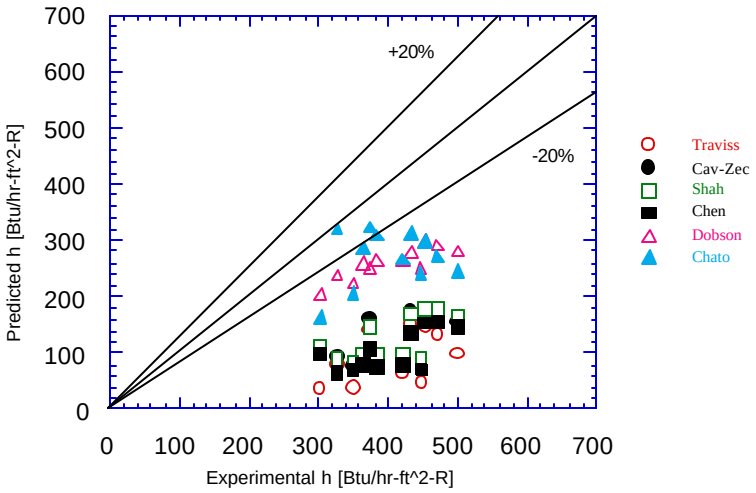

Figure 6.36 Predicted vs. Experimental Values of the Heat Transfer Coefficient for R-32/125 (5% Oil) at 55 and 110 klb/ft^2-hr (75 and 150 kg/m^2-s)--Properties Adjusted for Mixture Effects

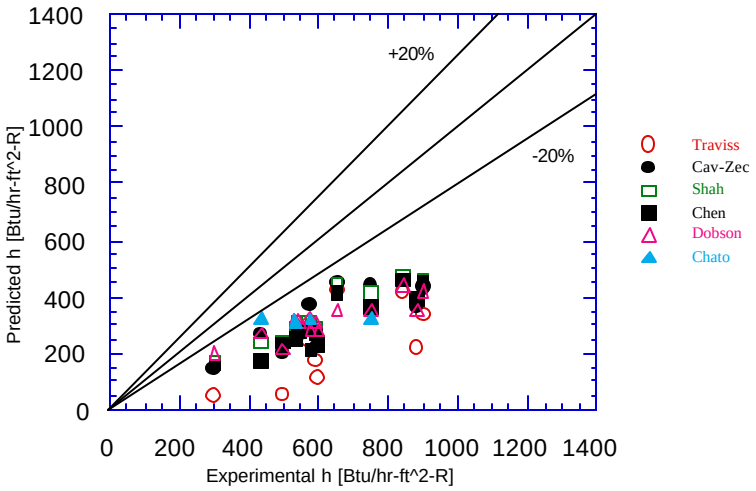

Figure 6.37 Predicted vs. Experimental Values of the Heat Transfer Coefficient for R-32/125 (5% Oil) at 220 and 364 klb/ft^2-hr (300 and 500 kg/m^2-s)--Properties Adjusted for Mixture Effects

To compare the experimental data with a correlation using a correction factor for oil addition, the Dobson correlation was chosen to be used with the oil correction factor proposed by Schlager et al. as mentioned in Chapter 2 (Equation 2.37). The graphed comparisons are shown in Figures 6.38 and 6.39, and show fairly good agreement at the low mass fluxes, though the calculated values consistently underpredict the experimental data by approximately 10%. At the higher mass fluxes the prediction shows more scatter, though on average predicts very accurately.

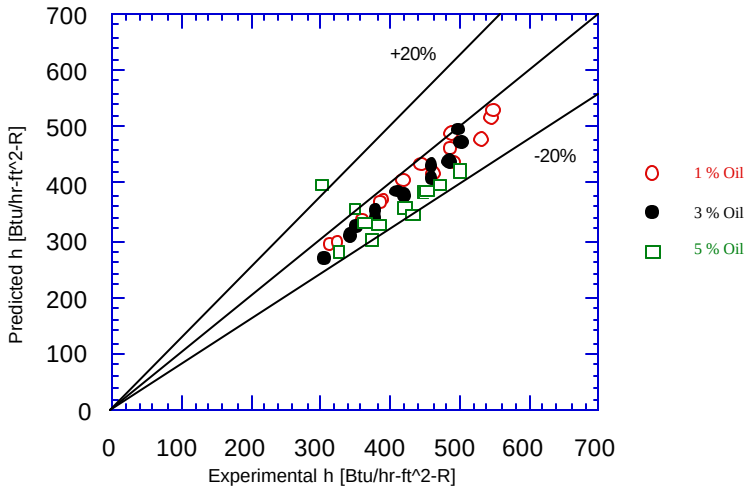

Figure 6.38 Experimental vs. Predicted h Using Correction Factor by Schlager et al. with Dobson Correlation at 55 and 110 klb/ft^2-hr (75 and 150 kg/m^2-s)

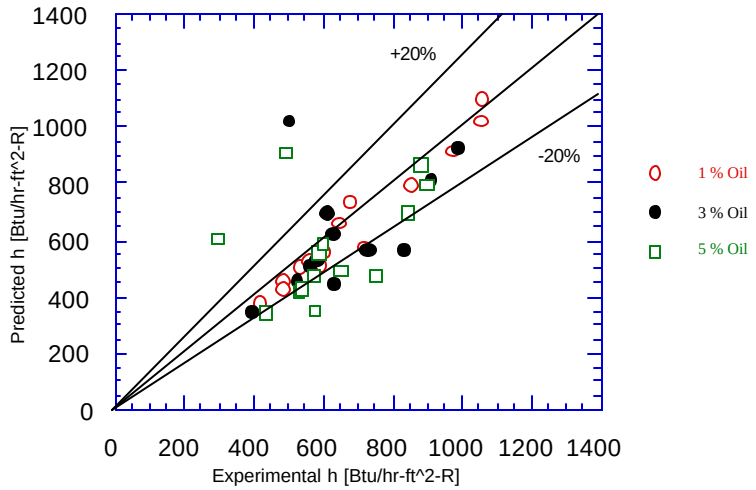

Figure 6.39 Experimental vs. Predicted h Using Correction Factor by Schlager et al. with Dobson Correlation at 220 and 364 klb/ft^2-hr (300 and 500 kg/m^2-s)

The experimental pressure drop for the oil-refrigerant mixtures is plotted versus vapor quality in Figure 6.40, and the pressure drop for the pure R-32/125 is superimposed on the graph as the solid and dashed lines. At the mass flux of 220 klb/ft^2-hr (300 kg/m^2-s) the pure data and the oil data seem to agree, though on average the oil-refrigerant mixture shows just slightly more pressure drop than the pure data. At the mass flux of 364 klb/ft^2-hr (500 kg/m^2-s), however, the oil-refrigerant mixtures show a significant increase in pressure drop compared to the pure refrigerant. A comparison between the experimental pressure drop and the predicted pressure drop using the Souza correlation for oil-refrigerant mixtures (Equation 2.41) is provided in Figure 6.41. This graph demonstrates that for qualities of $x<0.4$ the correlation overpredicts the experimental values by more than 20%, and for qualities of $x>0.9$ the correlation underpredicts the experimental data by more than 20%.

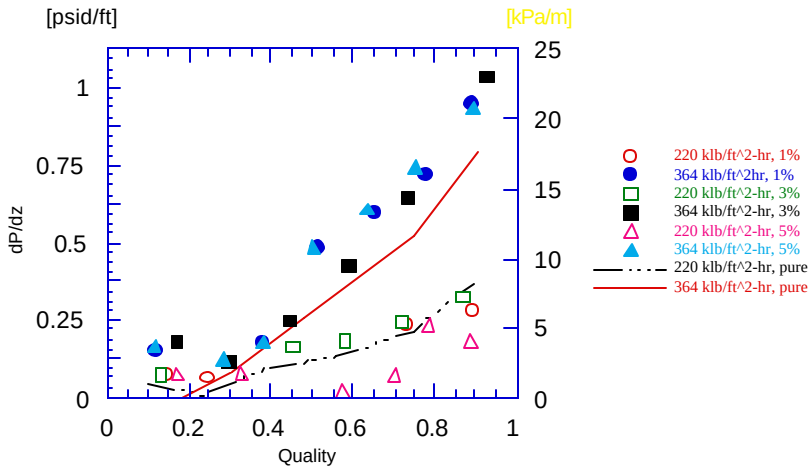

Figure 6.40 Experimental Pressure drop vs. Quality for Various Oil Concentrations

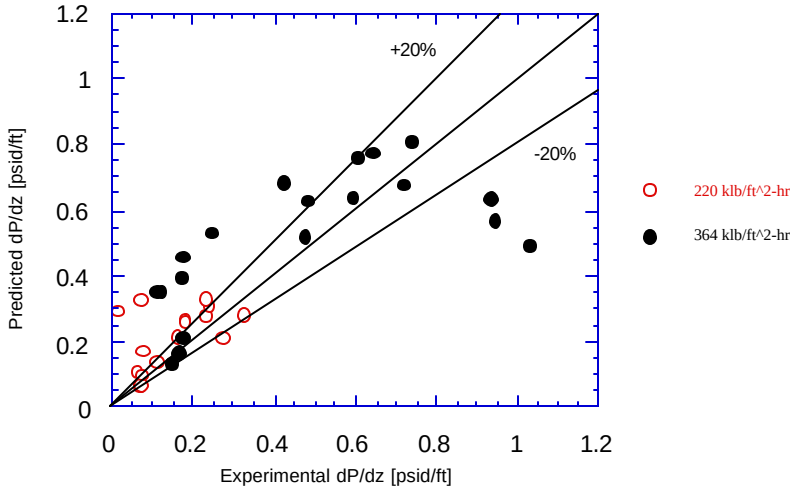

Figure 6.41 Predicted vs. Experimental Values of the Pressure Drop for R-32/125 Mixed with Oil Using the Souza Correlation

Chapter 7: Conclusions and Recommendations

The purpose of this work was to examine the effects of oil addition upon the heat transfer coefficient of R-32/125 undergoing condensation. The tests were performed for pure R-32/125 and ester oil concentrations of approximately 1%, 3%, and 5%. Pressure drop during condensation was also measured for both pure refrigerant and oil-refrigerant mixtures. This chapter summarizes the conclusions obtained from the results of this study, and proposes recommendations for future study.

7.1 Conclusions

The experimental values for the pure refrigerant show that the heat transfer coefficient increases monotonically with vapor quality. The slopes of the trends increase with increased mass flux. Of the six predictions examined for pure refrigerant, the Dobson correlation predicted the experimental data the best for both the low mass fluxes and the high mass fluxes, demonstrating its versatility regardless of flow regime. At the higher mass fluxes where the annular flow regime is encountered, the Cavalini-Zecchin and Traviss correlations also predict the experimental data fairly well. The pressure drop of the pure refrigerant tests showed steady increases with increased quality, though the Souza correlation predicts a decrease in pressure drop at very high qualities.

From the results of the oil-refrigerant mixture tests, the addition of oil causes a marked degradation in the heat transfer coefficient, especially at the higher mass fluxes over 110 klb/ft^2-hr (150 kg/m^2-s). This degradation tends not to be obvious until qualities of 50% or higher. The decrease in the heat transfer coefficient can be as great as 50% at qualities of 90%. After comparing the oil-refrigerant mixture data that was adjusted for apparent superheat effects with data that ignored the apparent superheat effects, it can be seen that the heat transfer coefficient may be measured to be 10% higher than what it actually is. The pure refrigerant correlations seem to predict the oil-refrigerant mixtures with close to the same accuracy as they predict the pure refrigerant tests if the oil properties are ignored. If the oil properties are included when using the correlations, the correlations do a very poor job of predicting the heat transfer coefficients. By using the Dobson correlation for pure refrigerants with the Schlager enhancement factor for oil-refrigerant mixtures in smooth tubes, the resulting correlation predicts the data very consistently to within 10%.

The pressure drop for oil-refrigerant mixtures was found to be as much as 20% higher than the pressure drop for the pure refrigerant. The correlation developed by Souza accurately predicts the pressure drop of the experimental data for qualities between 40% and 90%, though overestimates the data at low qualities and underestimates the data at high qualities.

The method of using a graph chromatography analyzer to measure the oil samples demonstrated to be fairly consistent at oil concentrations of 1% and 3%, though became fairly erratic at the 5% oil concentration. From the oil samples, it is concluded that the oil concentration of the mixture going through the test section will vary for different conditions even though the total amount of oil and refrigerant in the system remains constant. At different mass fluxes and vapor qualities the oil can collect in stagnant areas of the apparatus or wet the surfaces of areas where vapor is present. Therefore at higher mass fluxes the oil is circulated more uniformly.

7.2 Recommendations for Future Study

It is recommended that this subject be further investigated as follows:

1. More than one oil should be tested since the viscosities of oils vary and may have differing effects upon the heat transfer of the oil-refrigerant mixture.
2. Other refrigerants besides the R-32/125 azeotrope should be tested to observe if similar trends in the heat transfer and pressure drop are experienced. Such refrigerants could include R-22, R-134a, among others.
3. Other types of tubes should be tested, such as enhanced tubes with various internal fins.

As for recommended improvements for the experimental apparatus, the following is suggested:

1. More sensitive differential pressure transducers could be used because at the lower mass fluxes the measured pressure drop was often in the range of the uncertainty of the pressure transducers.
2. Construct "in-line" sampling ports to take oil samples. In this manner, a section of flow can be trapped to give a more accurate measurement of the oil concentration of the flow.

References

Akers, W. W., H. A. Deans, and O. K. Crosser, "Condensing Heat Transfer within Horizontal Tubes," American Institute of Chemical Engineers, Number 29, Vol. 55, 1959.

ASHRAE, "ANSI / ASHRAE Standard 41.4-1984: Standard Method for Measurement of Proportion of Oil in Liquid Refrigerant," American Society of Heating, Refrigerating and Air-Conditioning Engineers, Inc., 1984.

Baustian, J. J., M. B. Pate, and A. E. Bergles, "Properties of Oil-Refrigerant Mixtures with Applications to Oil Concentration Measurement: Part I—Thermophysical and Transport Properties," ASHRAE Transactions, Vol. 92, Part 1, pp. 55-73, 1986.

Bonhomme, D., "Condensation of Ozone-Safe Refrigerants in Horizontal Tubes: Experimental Test Facility and Preliminary Results," M.S. Thesis, University of Illinois at Urbana-Champaign, 1991.

Cavallini, Alberto and Roberto Zecchin, "A Dimensionless Correlation for Heat Transfer in Forced Convection Condensation," Proceedings of the Fifth International Heat Transfer Conference, Tokyo, Vol. 3, pp. 309-313, Sept. 3-7, 1974.

Cawte, Howard, "Effect of Lubricating Oil Contamination on Condensation in Refrigerant R22," International Journal of Energy Research, Vol. 16, pp. 327-340, 1992.

Chato, J. C., "Laminar Condensation Inside Horizontal and Inclined Tubes," ASHRAE Journal, Vol. 4, pg. 52, 1962.

Chen, S. L., F. M. Gerner, and C. L. Tien, "General Film Condensation Correlations," Experimental Heat Transfer, Vol. 1, pp. 93-107, 1987.

Chisholm, D., "The Influence of Mass Velocity on Friction Pressure Gradients During Steam-Water Flow," Engineering and Boiler House Rev., Vol. 78, No. 9, pp. 287-289, 1963.

Dobson, M. K., "Heat Transfer and Flow Regimes During Condensation in a Horizontal Tube," Doctoral Thesis, Department of Mechanical and Industrial Engineering, University of Illinois at Urbana-Champaign, 1994.

Eckles, S. J. and M. B. Pate, "In-Tube Evaporation and Condensation of Refrigerant-Lubricant Mixtures of HFC-134a and CFC-12," ASHRAE Transactions, Vol. 97, Part 2, 1991.

Eckles, S. J., S. C. Zoz, and M. B. Pate, "Using Solubility Data for HFC-134a and Ester Lubricant Mixtures to Model an In-Tube Evaporator or Condenser," ASHRAE Transactions, Vol. 99, Part 2, 1993.

Glas, Joseph P., "New Du Pont Position Stresses Orderly Transition to Alternatives," Fluorocarbon / Ozone Update, July, 1988.

Ha, s. and A. E. Bergles, "The Influence of Oil on Local Evaporation Heat Transfer Inside A Horizontal Microfin Tube," ASHRAE Transactions, Vol. 99, Part 1, 1993.

Hinde, D. K., M. K. Dobson, and J. C. Chato, "Condensation of Refrigerants 12 and 134a in Horizontal Tubes With and Without Oils," Air Conditioning and Refrigeration Center Technical Report Number 26, October, 1992.

Incropera, Frank P. and David P. De Witt, Fundamentals of Heat and Mass Transfer, Third Edition. John Wiley & Sons, Inc., New York, pp. 608-624, 1990.

Kedzierski, M. A., J.H. Kim, and D. A. Didion, "Causes of the Apparent Heat Transfer Degradation for Refrigerant Mixtures," ASME Two-Phase Flow and Heat Transfer, Vol. 197, 1992.

Moran, Michael J. and Howard N. Shapiro, Fundamentals of Engineering Thermodynamics. John Wiley & Sons, Inc., New York, 1988.

Reid, Robert C., John M. Prausnitz, and Bruce E. Poling, The Properties of Gases & Liquids, Fourth Edition. McGraw-Hill, Inc., United States, 1986.

Rohsenow, W. M. , J. H. Webber, and A. T. Ling, "Effect of Vapor Velocity on Laminar and Turbulent-Film Condensation," ASHRAE Transactions, Vol. 78, 1956.

Schlager, L. M., M. B. Pate, and A. E. Bergles, "Performance Predictions of Refrigerant-Oil Mixtures in Smooth and Internally Finned Tubes--Part I: Literature Review," ASHRAE Transactions, Vol. 96, Part 1, pp. 161-169, 1990.

Schlager, L. M., M. B. Pate, and A. E. Bergles, "Performance Predictions of Refrigerant-Oil Mixtures in Smooth and Internally Finned Tubes--Part II: Design Equations," ASHRAE Transactions, Vol.96, Part 1, pp. 170-182, 1990.

Shah, M. M., "A General Correlation for Heat Transfer during Film Condensation Inside Pipes," International Journal of Heat Mass Transfer, pp. 547-556, 1979.

Shah, M. M., "Heat Transfer during Film Condensation in Tubes and Annuli: A Review of the Literature," ASHRAE Transactions, Vol. 8, Part 1, 1981.

Soliman, H. M. and N. Z. Azer, "Flow Patterns During Condensation Inside a Horizontal Tube," ASHRAE Transactions, Vol. 77, Part 1, pp. 210-224, 1971.

Sur, B. and N. Z. Azer, "Effect of Oil on Heat Transfer and Pressure Drop During Condensation of Refrigerant-113 Inside Smooth and Internally Finned Tubes," ASHRAE Transactions, Vol. 97, Part 1, pp. 365-373, 1991.

Tichy, J. A., N. A. Macken, and W. M. B. Duval, "An Experimental Investigation of Heat Transfer in Forced Convection Condensation of Oil-Refrigerant Mixtures," ASHRAE Transactions, Vol. 91, Part 1A, pp. 297-303, 1985.

Traviss, D.P., W. M. Rohsenow, and A.B. Baron, "Forced Convection Condensation Inside Tubes: A Heat Transfer Equation for Condenser Design," ASHRAE Transactions, Vol. 79, Part 1, pp. 157-165, 1973.

Zivi, S. M., "Estimation of Steady-State Steam Void-Fraction by Means of the Principle of Minimum Entropy Production," Journal of Heat Transfer, ASME, Vol. 86, pg. 247, 1964.

Appendix A: Thermodynamic and Transport Properties of R-32/125

The sources used to obtain the thermodynamic and transport properties for the 50-50 mix of R-32/125 are Allied-Signal and the National Institute of Standards and Technology (NIST). Allied-Signal is the producer and supplier of the refrigerant used in this study, and the company provided data tables for the thermodynamic properties such as the saturation pressure and temperature relations as well as the densities and enthalpies for the liquid and vapor phases of the refrigerant for various saturation temperatures. The transport properties of the refrigerant are obtained using the computer program, *Refprops 3.0*, developed by NIST. The curve fits of the thermodynamic and transport properties are shown in Table A.1:

Table A.1 Curve Fits of Thermodynamic and Transport Properties for Pure R-32/125

Property	Curve Fit	Units
Tsat(P)	=(-14.965435+ln(P)+((14.965435-ln(P))^2 +6.3475433)^0.5)/0.001371392-273.15	[C]
Liquid Density	=1173.5798949-4.7094240934*T +0.0357252625*T^2-0.000921725219*T^3	[kg/m^3]
Vapor Density	=30.67+0.650569*T+0.047488452*T^2 -0.00108008*T^3+0.000013663458*T^4	[kg/m^3]
Liquid Enthalpy	=67.25293+1.5454435*T+0.011058846*T^2 -0.000371664*T^3+4.634192e-6*T^4	[kJ/kg]
Vapor Enthalpy	=224.0903-1.15937*T-0.01765698*T^2 +0.0004950496*T^3-6.2767169e-6*T^4	[kJ/kg]
Liquid Specific Heat	=1.2799+0.00110965*T+3.882943e-5*T^2 -6.437024e-7*T^3+1.226394e-8*T^4	[kJ/kg-K]
Liquid Viscosity	=2126.294-23.64835*T-0.1364137*T^2 +0.007068875*T^3-6.57250615e-5*T^4	[Micro Poise]
Vapor Viscosity	=118.791+0.621443*T-0.00485236*T^2 +0.0001712356*T^3	[Micro Poise]
Liquid Thermal Cond.	=0.11118-0.000748959*T-1.8657864e-6*T^2 +3.1228179e-10*T^3	[W/m-K]
Vapor Thermal Cond.	=0.0109494+6.15588e-5*T-3.8153e-7*T^2 +7.5594585e-9*T^3	[W/m-K]

Appendix B: Experimental Data

Table B.1 Experimental Data for Pure R-32/125

Mass Flux [klb/ft^2-hr]	X [%]	?X [%]	DTwall [R]	H [Btu/hr-ft^2-R]
55	12%	19%	5.17	247.27
55	24%	24%	5.17	317.19
55	40%	28%	5.24	372.14
55	51%	31%	5.27	403.84
55	66%	33%	5.31	435.37
55	78%	36%	5.60	457.38
110	8%	10%	5.35	259.95
110	28%	15%	5.36	411.06
110	41%	17%	5.27	474.29
110	55%	18%	5.26	521.14
110	71%	21%	5.51	560.94
110	85%	21%	5.22	632.80
220	10%	7%	5.38	367.03
220	23%	9%	5.36	482.74
220	39%	10%	5.38	558.48
220	56%	11%	5.58	615.54
220	75%	13%	5.45	707.83
220	89%	14%	5.09	828.82
364	18%	6%	5.27	527.48
364	30%	7%	5.36	639.84
364	48%	9%	5.60	805.75
364	75%	11%	5.00	1094.76
364	90%	13%	5.38	1165.03

Table B.2 Experimental Data for R-32/125 with 0.9% Oil

Mass Flux [klb/ft^2-hr]	X [%]	?X [%]	DTwall [R]	H [Btu/hr-ft^2-R]
55	19%	21%	4.94	314.21
55	31%	27%	5.31	360.62
55	42%	29%	5.35	391.03
55	52%	30%	5.13	418.98
55	62%	30%	4.92	445.95
55	72%	32%	4.75	487.19
55	82%	33%	4.96	488.70
110	14%	13%	5.85	324.11
110	28%	15%	5.45	386.12
110	39%	16%	5.14	461.93
110	50%	19%	5.56	492.53
110	62%	19%	5.19	530.62
110	77%	20%	5.21	546.59
110	86%	21%	5.62	549.49
220	14%	8%	5.56	421.35
220	25%	8%	4.67	486.93
220	35%	9%	4.74	534.41
220	45%	10%	5.07	564.60
220	59%	12%	5.59	607.23
220	73%	13%	5.61	648.17
220	90%	14%	5.60	685.03
364	12%	6%	5.63	486.07
364	24%	7%	5.62	597.48
364	38%	8%	5.66	722.92
364	51%	10%	5.31	854.42
364	65%	10%	5.01	979.40
364	78%	12%	5.15	1054.78
364	89%	12%	5.32	1060.19

Table B.3 Experimental Data for R-32/125 with 2.8% Oil

Mass Flux [klb/ft^2-hr]	X [%]	?X [%]	DTwall [R]	H [Btu/hr-ft^2-R]
55	20%	23%	5.41	307.16
55	32%	27%	5.52	344.56
55	41%	27%	4.95	379.06
55	50%	32%	5.86	378.99
55	62%	32%	5.52	411.71
55	79%	34%	5.22	458.75
110	20%	13%	5.23	352.75
110	33%	16%	5.42	422.21
110	43%	17%	5.33	459.46
110	56%	19%	5.59	485.05
110	69%	19%	5.52	503.35
110	85%	21%	6.19	498.71
220	13%	8%	5.77	396.23
220	30%	8%	4.62	528.79
220	45%	9%	4.84	566.28
220	58%	11%	5.34	586.23
220	72%	12%	5.55	632.89
220	87%	12%	5.76	618.73
364	17%	8%	5.95	637.18
364	30%	8%	5.26	731.91
364	45%	9%	5.32	834.67
364	59%	11%	5.73	913.26
364	73%	11%	5.35	991.61
364	93%	10%	9.58	505.61

Table B.4 Experimental Data for R-32/125 with 5.5% Oil

Mass Flux [klb/ft^2-hr]	X [%]	?X [%]	DTwall [R]	H [Btu/hr-ft^2-R]
55	29%	24%	5.37	327.21
55	44%	27%	5.04	382.89
55	51%	30%	5.91	364.05
55	62%	34%	5.86	421.40
55	73%	35%	5.61	447.16
55	77%	39%	8.10	350.74
110	21%	13%	5.51	372.83
110	34%	16%	5.43	433.68
110	48%	16%	5.27	453.21
110	58%	19%	6.03	470.85
110	70%	20%	5.89	499.59
110	86%	20%	9.36	303.00
220	17%	8%	5.60	437.15
220	33%	9%	5.08	533.64
220	44%	12%	6.52	542.59
220	57%	11%	5.82	574.82
220	70%	12%	5.90	592.04
220	79%	13%	6.18	601.22
220	89%	12%	11.59	300.23
364	12%	7%	6.11	578.13
364	28%	8%	5.15	751.40
364	38%	8%	5.98	654.73
364	50%	9%	5.30	843.60
364	64%	9%	5.02	899.84
364	75%	10%	5.38	882.62
364	90%	10%	9.73	496.14